Ca^{2+}-sensing receptor-mediated regulation of volume-sensitive Cl^- channels in human epithelial cells

Takahiro Shimizu

Department of Physiological Sciences

School of Life Science

The Graduate University for Advanced Studies

And

Department of Cell Physiology

National Institute for Physiological Sciences

Okazaki 444-8585, Japan

1999

SUMMARY

Since extracellular Ca^{2+} has been reported to modulate swelling-activated Cl^- currents, I examined an involvement of G protein-coupled Ca^{2+}-sensing receptor (CaR) in the regulation of the volume-sensitive Cl^- channel by reverse transcriptase polymerase chain reaction (RT-PCR), immunoblotting and whole-cell patch-clamp techniques, in a human epithelial cell line (Intestine 407).

RT-PCR confirmed that the Intestine 407 cell contains mRNAs cording for the CaR, and expression of the CaR protein was evidenced by immunoblotting analysis. The swelling-activated whole-cell Cl^- current was augmented by addition of Ca^{2+} to the bathing solution in a concentration-dependent manner. The total Ca^{2+} concentration for half-maximal stimulation (EC_{50}) was 6.5 mM. A rise in the extracellular Mg^{2+} concentration also concentration-dependently increased the amplitude of volume-sensitive Cl^- currents, though less effective (EC_{50} of around 22 mM) than Ca^{2+}. In addition, other CaR agonists, La^{3+} (3 μM), neomycin (500 μM) and spermine (1 mM), significantly augmented the Cl^- current. To further confirm an involvement of the CaR in the upregulating effect of extracellular Ca^{2+} on the volume-sensitive Cl^- current, I examined the effects of GDPβS, which is a G protein inhibitor, and GTPγS, which is a G protein activator, on the Cl^- current. Incorporation of GDPβS in the pipette (intracellular) solution abolished extracellular Ca^{2+}-induced enhancement of the Cl^- current. Under Ca^{2+}- and Mg^{2+}-free conditions, the amplitude of volume-sensitive Cl^- currents became increased by the presence of intracellular GTPγS. Further augmentation was never induced by addition of extracellular Ca^{2+} in the presence

of intracellular GTPγS. These results demonstrate that the G protein-coupled CaR mediates Ca^{2+}-induced upregulation of the volume-sensitive Cl^- channel in Intestine 407 cells.

I then investigated the signal transduction pathway of CaR-mediated regulation of volume-sensitive Cl^- channel. The augmenting effect of extracellular Ca^{2+} on the Cl^- current could be abolished neither by application of 1,2-bis(2-aminophenoxy)ethane-N,N,N',N'-tetraacetic acid (BAPTA: 5 mM) to the pipette (intracellular) solution nor by 24 h-pretreatment with purtussis toxin (PTX: 100 ng/ml). When the intracellular cAMP concentration was elevated by application of a cocktail of forskolin (10 μM), dibutylyl cAMP (1 mM) and 3-isobutyl-1-methylxanthine (IBMX: 400 μM), the amplitude of volume-sensitive Cl^- current was markedly enlarged. Under the cAMP stimulation, extracellular Ca^{2+} failed to increase the Cl^- current. These results suggest that the CaR is coupled to Gs and modulates the volume-sensitive Cl^- channel via an increase in intracellular cAMP level.

Effects of CaR stimulation on volume sensitivity of swelling-activated whole-cell Cl^- current was then assessed. When the whole-cell Cl^- current density was plotted against the relative cell surface area measured simultaneously, the data points were well fitted to the Boltzmann function. Elevation of extracellular Ca^{2+} shifted the curve to the left and increased the slope. These results indicate that CaR-mediated augmentation of the Cl^- channel is due to increased sensitivity of the channel (or its accessory volume sensor) to cell volume expansion.

Extracellular Ca^{2+} or Mg^{2+} exhibited an additional effect on the volume-sensitive Cl^- current: facilitation of its depolarization-induced

inactivation kinetics. The inactivation time course of the Cl^- current at large positive potentials became faster in the presence of extracellular Ca^{2+} or Mg^{2+}. The relative half inactivation time at +100 mV was maximally decreased to 60.4 and 40.7% by Ca^{2+} and Mg^{2+}, respectively. In contrast to the effects on the Cl^- current amplitude, EC_{50} of the Mg^{2+} effect on the inactivation kinetics (2.1 mM) was smaller than that of the Ca^{2+} effect (2.5 mM). In addition, all other CaR agonists examined failed to accelerate the inactivation time course. Furthermore, the extracellular Ca^{2+} effect on inactivation kinetics was not affected by GDPβS or GTPγS. These results indicate that the CaR does not mediate the effect of extracellular Ca^{2+} or Mg^{2+} on the depolarization-induced inactivation kinetics.

Taken together, it is concluded that stimulation of CaR induces upregulation of volume-sensitive Cl^- channels by enhancing the volume expansion sensitivity in human epithelial Intestine 407 cells. The second messenger is likely to be cAMP but not Ca^{2+} in the cytosol. The accelerating effect of extracellular divalent cations on inactivation time course of the Cl^- current is induced by a different mechanism without mediation by the CaR.

INTRODUCTION

Cell volume regulation is an essential function for animal cells, because osmotic perturbation is coupled to a variety of physiological and pathological processes, such as cell proliferation, differentiation and cell death (for reviews see Lang, 1998, Lang et al., 1998, Okada, 1998). Under extracellular hypotonic conditions, cells are swelled by an influx of water. Soon after such osmotic cell swelling, numerous cell types can recover their original cell volume by regulatory volume decrease (RVD) mechanism. The RVD is accomplished by net efflux of electrolytes, organic solute, and water as a consequence of activation of a set of channels and transporters. Volume-sensitive Cl^- channels are responsible for anion efflux during RVD in most cell types. Up to now, properties of the volume-sensitive Cl^- channel have been extensively studied in many cell types, as summarized in a recent review (Okada, 1997). The phenotypic properties of the major volume-sensitive Cl^- channel which is expressed in a large variety of cell types have been well characterized by moderate outward rectification, intermediate single-channel conductance, a low-field anion selectivity, time-dependent inactivation at large positive potentials, and intracellular ATP dependency (see Strange et al., 1996; Nilius et al., 1997; Okada, 1997; Okada et al., 1998). However, the activation mechanism of the volume-sensitive outwardly rectifying (VSOR) Cl^- channel remains as yet largely unknown.

In order to elucidate the activation mechanism, investigation of signaling machinery for modulation of VSOR Cl^- channel is of great importance. There are some reports about effects of extracellular Ca^{2+} on volume-sensitive Cl^- currents.

First, the time course and extent of inactivation of VSOR Cl^- currents were dependent on the extracellular cations. Divalent cations added in the bathing solution facilitated the inactivation kinetics at large positive potentials in human epithelial H69AR and HeLa S5 cells with the relative efficacy of $Mg^{2+} > Ca^{2+} > Sr^{2+} > Ba^{2+}$ (Anderson et al., 1995). A similar effect of extracellular Mg^{2+} was also observed in T84 cells (Braun & Schulman, 1996). Furthermore, an increase in the extracellular Ca^{2+} or Mg^{2+} concentration accelerated depolarization-induced inactivation in a mouse myoblast cell line (Voets et al., 1997). On the other hand, recently, Ca^{2+} in an extracellular medium was also reported to affect the amplitude of volume-sensitive Cl^- currents. In mouse osteoclasts, a rise in extracellular Ca^{2+} level was found to increase the swelling-activated Cl^- conductance by Sakai et al. (1999). However, the molecular mechanisms of these effects of extracellular divalent cations have not been investigated in detail.

Numerous physiological functions involve Ca^{2+} ions. Intracellular Ca^{2+} is a key messenger and cofactor for various enzymes. The resting free concentration cytosolic Ca^{2+} is below 100 nM but can increase over 1 μM upon cellular activation owing to release of Ca^{2+} from intracellular stores and/or uptake of Ca^{2+} from the extracellular milieu. In contrast, the extracellular Ca^{2+} concentration is ~10,000-fold higher than intracellular Ca^{2+} concentration and maintained virtually constant at ~1 mM. However, regulation of extracellular Ca^{2+} concentration within a narrow physiological range is crucial for a variety of cellular processes that include control of cellular proliferation, differentiation and secretion (Brown, 1991, Buras et al., 1995). Ca^{2+} plays several important roles in

intestinal functions. Intestinal epithelial cells mediate vitamine D-dependent Ca^{2+} absorption. Extracellular Ca^{2+} modulates resposiveness to vitamin D in intestinal epithelial cells (Giuliano & Wood, 1991). In addition, a high concentration of extracellular Ca^{2+} promotes differentiation of intestinal epithelial cells and decreases their growth by as yet undefined pathways (Boynton, 1988; Buras et al., 1995; Hulla et al., 1995), although a recent report suggests that activation of Ca^{2+}-sensing receptor (CaR) may be one of the steps in the pathway (Kallay et al., 1997).

From the bovine parathyroid, Brown and associates (1993) recently cloned a gene of CaR, which is a G protein-coupled transmembrane heptahelical receptor that senses extracellular divalent cations as an extracellular first messenger. In the topology model, the CaR has very large extracellular amino terminal that seems to bind divalent cations. The CaR is activated not only by divalent cations but also most trivalent cations with a rank order of potency: $La^{3+} > Gd^{3+} > Be^{2+} > Ca^{2+} = Ba^{2+} > Sr^{2+} > Mg^{2+}$ (see Nemeth, 1998). In addition to inorganic polycations, many organic polycations, such as polyamines (e.g. spermine) and aminoglycoside antibiotics (e.g. neomycin), also activate the CaR (Quinn et al., 1997; Brown et al., 1998). Interestingly, the CaR is expressed not only in the tissues involved in serum calcium regulation (such as the parathyroid, calcitonin-secreting cells of the thyroid, and the kidney) but also in a number of other tissues with functions unrelated directly to Ca^{2+} homeostasis (Butters et al., 1997; Brown et al., 1998). In many of these tissues, the physiological role of the CaR is not understood.

In the present study, I have tested a possibility that the CaR mediates

extracellular Ca^{2+}-induced modulation of VSOR Cl^- channels in human epithelial Intestine 407 cells by applying patch-clamp and molecular biological techniques. I have found two different effects of extracellular Ca^{2+} or Mg^{2+}: First, the VSOR Cl^- current was markedly increased, and second the depolarization-induced inactivation kinetics of the Cl^- channel were facilitated in Intestine 407 cells. On the other hand, organic polycations failed to accelerate inactivation kinetics, while they enhanced the VSOR Cl^- current. Intracellular application of GDPβS abolished the Ca^{2+} effect on the Cl^- current amplitude, but not that on the inactivation kinetics. These results indicate that in Intestine 407 cells the effect of extracellular Ca^{2+} on the Cl^- current amplitude is mediated by G protein-coupled CaR, whereas the mechanism by which extracellular Ca^{2+} facilitates the channel inactivation is independent of CaR. Furthermore, I have demonstrated that cAMP is the second messenger for CaR-mediated upregulation of VSOR Cl^- channel.

Materials and Methods

Cell culture

A human embryonic small intestinal epithelial cell line, Intestine 407, was cultured in monolayer in Fischer medium supplemented with 10% newborn bovine serum (Flow Labs Inc.), as described previously (Hazama & Okada, 1988). The cells attached on the plastic substrate were provided for reverse transcriptase polymerase chain reaction (RT-PCR) or immunoblotting studies. For patch-clamp studies, suspensions of spherical cells were prepared by mechanical detachment from the plastic substrate, as reported previously (Kubo & Okada, 1992). The suspensions were cultured with agitation for 15–300 min, and the cells were placed in a chamber (0.3 ml). After attaching to the glass substrate, the cells were perfused with bathing solutions at a flow rate of around 5 ml min^{-1}.

RNA isolation and RT-PCR

Poly $(A)^+$ RNA was extracted from Intestine 407 cells using Direct mRNA Purification Kit with magnetic porous glass (MPG) (CPG Inc., New Jersey, USA). Briefly, the cells were homogenized in extraction-hybridization buffer, which contained 100 mM Tris-HCl (pH 8.0), 500 mM LiCl, 10 mM EDTA, 1 % lithium dodecylsulphate (LiDS) and 5 mM dithiothreitol (DTT). Poly $(A)^+$ RNA was magnetically isolated from the homogenate by binding with MPG-bound oligo$(dT)_{25}$. The poly $(A)^+$ RNA of 400 ng was used for single-strand cDNA

synthesis using SuperScript Preamplification System (Life Technologies, Rockville, USA). In brief, RNA samples were reverse transcribed at 42℃ for 50 min by incubation with 20 μl of an RT mixture containing the following constituents: 500 ng of oligo$(dT)_{12\text{-}18}$, 20 mM Tris-HCl (pH 8.4), 50 mM KCl, 2.5 mM $MgCl_2$, 1 mM dNTPs, 10 mM DTT and 200 units of SuperScript II RT. The reverse transcriptase was then inactivated by heating at 70℃ for 15 min. The resultant first-strand cDNA was used for the PCR procedure. PCR was performed in a total volume of 50 μl of a buffer solution containing 20 mM Tris-HCl (pH 8.4), 50 mM KCl, 1.5 mM $MgCl_2$, 0.2 mM dNTPs and 250 units of Ampli Taq Gold (Perkin-Elmer, New Jersey, USA), using the following set of primers (200 nM each), which were based on the sequence of the human kidney CaR (HuKCaSR: Aida et al., 1995). The sense and antisense primer sequences were 5'-CACAATTGCAGCTGATGACG-3' and 5'-CTTCAGAGCGAATCCAA -TGG-3', respectively. The set of primers is predicted to yield a 340-bp product. The optimum temperature cycling protocol was determined to be 94℃ for 1 min, 52℃ for 1 min and 72℃ for 2 min for 2 rounds of 40 cycles using a programmable thermal cycler (GeneAmp PCR System 9600, Perkin-Elmer). Two sets of negative control experiments were performed by including primers but no cDNA or RNA that was not reverse transcribed. PCR products were directly subjected to sequencing using an ABI PRISM 310 automated sequencer (Perkin-Elmer).

Immunoblotting

Crude membranes from Intestine 407 cells were prepared by Dounce

homogenization followed by differential centrifugation. In brief, cells were twice washed with phosphate-buffered saline (PBS), collected by a cell scraper, and homogenized using 30 strokes of a homogenizer in 10 volume of homogenization buffer, which contained (in mM): 250 sucrose, 5 EDTA, 5 EGTA and 10 HEPES (pH 7.4). The resultant homogenate was centrifuged at 10,000 rpm for 30 min. The supernatant was subsequently centrifuged at 100,000 rpm for 2 h to pellet the microsomal fraction, and the resultant pellet was solubilized with sample buffer containing: 2% sodium dodecylsulfate (SDS), 10% glycerol, 0.063 mM Tris-HCl (pH 6.8), 0.002% Bromophenol Blue and 5% 2-mercaptoethanol. All steps were carried out at 4℃.

An aliquot of 30 μg of membrane protein was subjected to SDS-polyacrylamide gel electrophoresis (SDS-PAGE) using a 7.5% polyacrylamide gel. The proteins on the gel were electrophoretically transferred to nitrocellulose sheets, which were subsequently incubated for 1 h with 1:1,000 dilution of affinity-purified polyclonal antibody (Affinity Bioreagents, Inc, USA) raised against a peptide corresponding to amino acids 12–27 of the rat kidney CaR. The purified rabbit IgG was substituted for the primary antibody for negative control experiments. Antibody detection was performed using an Amersham biotin-streptavidin system with biotinylated anti-rabbit Ig and nitro blue tetrazolium–5-bromo-4-chloro-3-indolyl phosphate (NBT–BCIP) system (Amersham Life Science, Little Chalfont, UK).

Patch-clamp experiments

Whole-cell recordings were performed, as reported previously (Kubo & Okada,

1992; Liu et al., 1998), The patch electrodes were fabricated from borosilicate glass capillaries (outer diameter=1.4 mm, inner diameter=1.0 mm, Asahi Rika-Glass Industry, Japan) using a micropipette puller (P-2000, Sutter Instrument, USA). The wide-tipped electrodes had a resistance of around 2 MΩ, when filled with pipette solution. Series resistance (<5 MΩ) was compensated (to 70–80%) to minimize voltage errors. Currents were recorded using an Axopatch 200A amplifier (Axon Instruments, Foster City, CA). Current signals were filtered at 1 kHz using a four-pole Bessel filter and digitized at 4 kHz. The pClamp software (version 6.0.2; Axon Instruments) was used for command pulse control, data acquisition and analysis. The time course of current activation and recovery was monitored by repetitively applying (every 15 s) alternating step pulses (2 s duration) from a holding potential of 0 mV to ±40 mV. To observe voltage dependence of the current profile especially inactivation kinetics at large positive potentials, stepping pulses (2 s duration) were applied from a prepotential at −100 mV to test potentials of −80 to +100 or +120 mV in 20-mV increments after attaining steady activation of swelling-induced current. The amplitude of instantaneous current was measured at 1.25 ms after the step pulse onset. The steady-state current level was evaluated by fitting the time course of inactivation to a double exponential function, when inactivation kinetics were analyzed. To evaluate concentration dependency of Ca^{2+} or Mg^{2+} on the overall profile of inactivation kinetics, the half-inactivation time was calculated as the time to reach the 50% inactivation of the Cl^- current recorded at +100 mV.

The control isotonic external solution contained (in mM): 110 CsCl, 12

HEPES, 7 Tris, and 110 mannitol (pH 7.4, 330 mosmol kg-H_2O^{-1}). The control hypotonic solution were made by reducing the concentration of mannitol to 50 mM (pH 7.4, 270 mosmol kg-H_2O^{-1}). The osmolality of solutions was measured using a freezing-point depression osmometer (OM802, Vogel, Germany). In some experiments, 110 mM CsCl was replaced with 110 mM KCl. The Ca^{2+}- or Mg^{2+}- containing solutions (0.1–55.0 mM) were prepared by substituting $CaCl_2$ or $MgCl_2$ for CsCl with maintaining the total Cl^- concentration constant and with adjusting the osmolality by adding appropriate amount of mannitol. The pipette (intracellular) solution contained (in mM): 110 CsCl, 2 $MgSO_4$, 1 Na_2-ATP, 15 Na-HEPES, 10 HEPES, 1 ethylene glycol bis(β-aminoethylether)-N,N,N',N'-tetraacetic acid (EGTA), and 40 mannitol (pH 7.3, 290 mosmol kg-H_2O^{-1}). The osmolality of the pipette solution was set lower (by 40 mosmol kg-H_2O^{-1}) than that of the control isotonic bathing solution in order to prevent spontaneous cell swelling after attaining the whole-cell mode (due to poorly diffusible cytosolic constituents: Worrell et al., 1989). When necessary, 5 mM 1,2-bis(2-aminophenoxy)ethane-N,N,N',N'-tetraacetic acid (BAPTA) was substituted for EGTA.

Cell size measurements

During whole-cell current recordings, cell size in isotonic and hypotonic conditions was simultaneously measured by monitoring with a CCD camera (ICD-42AC, Ikegami, Tokyo, Japan), as reported previously (Miwa et al., 1997). Two-dimensional cell size was evaluated by the square of diameter of the spherical cell contour morphology. When the membrane blebs were found, the

data were discarded. However, the data were accepted after fusion of a number of blebs gave rise to rounding the cell. The relative surface area was calculated by normalizing the cell size under hypotonic conditions against the steady-state cell size under isotonic conditions.

Chemicals

All the agents except for EGTA, forskolin (Wako, Osaka, Japan), Na-HEPES (Nacalai Tesque, Kyoto, Japan) and purtussis toxin (PTX: Calbiochem, CA, USA) were obtained from Sigma (St. Louis, USA). GDPβS, GTPγS and PTX were added to pipette (intracellular) solutions. The stock solution of neomycin was prepared just before use, because neomycin is sensitive to light. Forskolin and phloretin were dissolved in ethanol as the stock solution and diluted 1,000 times in the corresponding bathing solution. 3-Isobutyl-1-methylxanthine (IBMX) was dissolved in dimethyl sulfoxide as the stock solution and diluted 1,000 times in the corresponding bathing solution. The vehicle (ethanol and dimethyl sulfoxide) alone at the employed concentration (0.1%) did not affect the VSOR Cl^- current.

Statistical analysis

All experiments were carried out at room temperature (22–26℃). Data are given as means ± S.E.M of observations (n). Statistical differences of the data were evaluated by Student's paired or unpaired t-test and considered significant at $P < 0.05$.

RESULTS

RT-PCR analysis of expression of the CaR gene

Expression of the CaR gene has not been previously established in cultured Intestine 407 cells. Therefore RT-PCR was performed on RNA isolated from Intestine 407 cells to examine expression of the CaR gene. Figure 1 shows results of RT-PCR amplification. As shown in Fig. 1A, the PCR product of the expected length, i.e., 340 base pair, was amplified by CaR-specific primers from reverse-transcribed RNA (*lane 2*). However, no PCR product was amplified when the cDNA (data not shown) or the reverse transcriptase (*lane 3*) was omitted from the reaction. Figure 1B illustrates the nucleotide sequence of an RT-PCR product. The PCR product sequence was aligned with the sequence of the human kidney CaR (HuKCaSR) cDNA clone. The nucleotide sequence of the PCR product revealed >99% identity with the corresponding region of HuKCaSR, as shown in Fig. 1B. However, the resultant amino acid sequence of the CaR was not different between each other.

Expression of the CaR protein as assessed by Western immunoblot

In order to detect expression of the CaR protein, Western immunoblotting was performed using a polyclonal anti-CaR antibody in Intestine 407 cells. As shown in Fig. 2, immunoblotting of cell membrane preparation revealed strong CaR staining (*lane 1*). The major immunoreactive band detected in the Intestine 407 lysates had a molecular mass of around 110 kDa. In contrast, the major band was not observed, when the nitrocellulose sheet was reacted to control rabbit IgG

(*lane 2*).

Effects of extracellular Ca^{2+} on volume-sensitive Cl^- currents

Outwardly rectifying whole-cell Cl^- currents were activated in Intestine 407 cells by exposure to hypotonic solution (82% osmolality) under Ca^{2+}- and Mg^{2+}-free conditions. After the VSOR Cl^- current reached a saturated level, effects of extracellular Ca^{2+} on the VSOR Cl^- currents were observed. Figure 3A shows a representative record. An increase in extracellular Ca^{2+} concentration to 10 mM remarkably augmented the VSOR Cl^- current recorded at ±40 mV in a reversible manner. As shown in Fig. 3B, extracellular Ca^{2+} augmented instantaneous currents even when time-dependent inactivation was prominently induced by large positive potentials. The instantaneous current-voltage (I-V) relationships shows that the extracellular Ca^{2+} effect on the Cl^- current was observed in the wide voltage range up to ±100 mV, as shown in Fig. 3C. In contract, under isotonic conditions, a rise in the extracellular Ca^{2+} concentration did not affect basal Cl^- currents (n=7, data not shown). Furthermore, phloretin (300 μM), which is known to block specifically the volume-sensitive Cl^- current in Intestine 407 cells (Fan et al., 1999), completely inhibited the VSOR Cl^- current both in the absence and presence of extracellular Ca^{2+} (n=3, data not shown). Replacement of Cs^+ with K^+ in the bathing solution never affected the VSOR Cl^- current (n=10, data not shown). These results demonstrate that extracellular Ca^{2+} but not K^+ modulates the VSOR Cl^- current. The upregulating effect of extracellular Ca^{2+} on the amplitude of instantaneous current was concentration-dependent, as depicted in Fig. 4. The total Ca^{2+} concentration for

half-maximal activation (EC_{50}) was 6.5 ± 0.2 mM at –40 mV.

Extracellular Ca^{2+} also accelerated the inactivation time course of the Cl^- currents at large positive potentials (Fig. 3B). The time course of inactivation could be fitted to a double exponential function, as reported previously (Tsumura et al., 1996; Liu et al., 1998). Figure 5A shows representative data of the fitting at +120 mV. As shown in Fig. 5 (B & C), both the fast and slow time constants (τ_f and τ_s) were significantly decreased by a high concentration of extracellular Ca^{2+} (55 mM) at positive potentials to +80 mV. To assess concentration dependency of the effect of extracellular Ca^{2+} on the inactivation process, the half-inactivation time was then calculated (see *Materials and Methods*). As shown in Fig. 6, the relative half inactivation time at +100 mV was concentration-dependently decreased. The maximum inhibition was 60.4 ± 0.01%, and the EC_{50} 2.5 ± 0.01 mM.

Effects of extracellular Mg^{2+} on volume-sensitive Cl^- currents

Effects of another divalent cation, Mg^{2+}, on the VSOR Cl^- current were next examined. As shown in Fig. 7, an increase in the extracellular Mg^{2+} concentration to 20 mM significantly augmented the VSOR Cl^- current. The effect of Mg^{2+} was reversible. Figure 8 shows the concentration-activation relationship for the instantaneous current. The effect of Mg^{2+} was less potent than that of Ca^{2+}, and the EC_{50} was estimated to be 22.0 ± 0.5 mM at –40 mV. Since Mg^{2+} is known to be a less potent agonist of the CaR than Ca^{2+} (Brown et al., 1993), these data are compatible with the hypothesis that the CaR is involved in the effect of extracellular divalent cations on the VSOR current amplitude.

As shown in Figs. 7B and 9A, extracellular Mg^{2+} had the accelerating effect on the inactivation process of the VSOR Cl^- current. As shown in Fig. 9 (B & C), both τ_f and τ_s values were significantly reduced by Mg^{2+} at +80 to +120 mV. Figure 10 depicts the relationship between the extracellular Mg^{2+} concentration and the half inactivation time observed at +100 mV. The maximum inhibition was 40.7 ± 0.01% and the EC_{50} 2.1 ± 0.1 mM. Thus, the rank order of potency of Ca^{2+} and Mg^{2+} for the accelerating effect on inactivation kinetics was opposite to that for the augmenting effect on instantaneous currents.

Effects of the CaR agonists on volume-sensitive Cl^- currents

To determine whether the CaR actually modulates the VSOR Cl^- current, other established agonists of the CaR were examined. Trivalent cations (e.g. La^{3+}) and organic polycations (e.g. neomycin and spermine) are known to activate the CaR (Brown et al., 1998). Figure 11 illustrates effects of La^{3+} on the VSOR Cl^- currents. Application of 3 μM La^{3+} to hypotonic Ca^{2+}- and Mg^{2+}-free bathing solution significantly increased the instantaneous Cl^- current, although the effect of La^{3+} was not reversible (Fig. 11A). Figures 12 and 13 show effects of neomycin and spermine on the Cl^- current, respectively. Both neomycin (500 μM) and spermine (1 mM), which were added to hypotonic Ca^{2+}- and Mg^{2+}-free bathing solutions, induced increases in the VSOR Cl^- current amplitude in a reversible manner (Figs. 12A & 13A). Effects of La^{3+}, neomycin and spermine were observed in the entire voltage range examined (Figs. 11C, 12C & 13C). These results demonstrated that the VSOR Cl^- current is augmented by a variety of CaR agonists.

The time course of depolarization-induced inactivation was, however, little affected by these cations, in contrast to Ca^{2+} and Mg^{2+}, as shown in Figs. 11B, 12B & 13B. To analyze in detail, inactivation time constants were calculated. Figure 14 shows the effect of neomycin on inactivation time constants at +100 mV. Both τ_f and τ_s values in the presence of neomycin were not significantly different from those in the absence of neomycin. Essentially same results were obtained for the effects of La^{3+} and spermine (n=5–9, data not shown). These results indicate that the accelerating effect of these cations on depolarization-induced inactivation kinetics was not mediated by the CaR.

G protein involvement in the upregulating effect of extracellular Ca^{2+}

The upregulating effect of extracellular Ca^{2+} on the VSOR Cl^- channel would be mediated by activation of GTP-binding proteins (G proteins), because the CaR is a G protein-coupled receptor. To further confirm that the effect of extracellular Ca^{2+} is due to stimulation of the CaR, I examined whether G proteins are involved in the activation mechanism. Figure 15 shows the effects of the inhibitor, GDPβS, and the activator, GTPγS, added to pipette (intracellular) solution on the instantaneous VSOR Cl^- current under Ca^{2+}- and Mg^{2+}-free conditions. Both GDPβS and GTPγS never affected the basal Cl^- current observed under isotonic conditions. However, GTPγS markedly increased the VSOR Cl^- current, whereas GDPβS little affected the current. In contrast, both GDPβS and GTPγS did not affect the inactivation kinetics of VSOR Cl^- currents at large positive potentials, as shown in Fig. 16. In the presence of 500 μM GDPβS, an increase in extracellular Ca^{2+} concentration to 10 mM failed to augment significantly the

VSOR Cl^- current, as shown in Fig. 17. However, extracellular Ca^{2+} accelerated the inactivation process at large positive potentials (Fig. 17B). As shown in Fig. 18, application of 500 μM GTPγS to pipette solution also abolished the extracellular Ca^{2+} effect on the VSOR Cl^- current. However, the accelerating effect of Ca^{2+} on the inactivation was preserved, as shown in Fig. 18B. These results demonstrate the upregulating effect, but not the accelerating effect, of extracellular Ca^{2+} was mediated by activation of G proteins. These results provide additional evidence for the hypothesis that the G protein-coupled CaR is involved in the upregulating effect of extracellular Ca^{2+} on the instantaneous VSOR Cl^- current but not in the accelerating effect on the inactivation kinetics.

Pertussis toxin (PTX) inhibits the coupling of Gi or Go to receptors by ADP-ribosylating the α subunit of these G proteins. To test an involvement of Gi or Go, cells were preincubated for 24 h with 100 ng/ml PTX added to the culture medium, and PTX was also added to pipette solution during whole-cell recordings. As shown in Fig. 19, PTX failed to inhibit the Ca^{2+}-induced increase in the VSOR Cl^- current. This result suggests that the G protein coupled to the CaR is not Gi or Go.

cAMP as the second messenger

Furthermore, I examined the second messenger involved in the signal transduction pathway between the CaR and the VSOR Cl^- channel. It has been reported that a variety of second messengers, including intracellular Ca^{2+} and cAMP, are involved in the CaR signaling (see Nemeth, 1998). First, the possibility that intracellular Ca^{2+} is the second messenger for extracellular

Ca^{2+}-induced activation of the VSOR Cl^- current was tested. Figure 20 shows effects of 5 mM BAPTA added to pipette solution. Even in the presence of this Ca^{2+} chelator, the VSOR Cl^- current was remarkably increased by extracellular Ca^{2+}, indicating that the activation effect of Ca^{2+} on the Cl^- current is not dependent on the cytoplasmic free Ca^{2+} concentration. Second, the possibility that intracellular cAMP exerts the messenger action was investigated. To elevate the intracellular cAMP concentration, a cocktail of forskolin (10 μM), dibutylyl cAMP (1 mM) and IBMX (400 μM) was used. As shown in Fig. 21, after steady-state activation by hypotonic Ca^{2+}- and Mg^{2+}-free solution, the VSOR Cl^- current was remarkably increased by cAMP. Extracellular Ca^{2+} failed to augment further the Cl^- current, when the intracellular cAMP level was raised. This result indicates that cAMP acts as the second messenger downstream the CaR, and suggests that the CaR is coupled to Gs.

Effects of extracellular Ca^{2+} on volume expansion sensitivity of the VSOR Cl^- channel

Volume expansion sensitivity was assessed by plotting the VSOR Cl^- current against the relative surface area measured simultaneously, as reported previously (Miwa et al., 1997), because the current density could be better fitted to the second power of the cell diameter than to the first or third power to Boltzmann's equation (Shimizu et al., 1999):

$$y = \frac{A_1 - A_2}{1 + e^{(x - x_0)/q}} + A_2$$

where x_o is the half activation energy, and q a slope factor. As shown in Fig. 22A,

a rise in extracellular Ca^{2+} concentration to 55 mM increased the slope of the current density change in response to the change in the relative surface area. Each set of data collected from the same cell could be well fitted to the Boltzmann function, and Figure 22B shows the representative fitting of the data with and without extracellular Ca^{2+}. By an increase in the extracellular Ca^{2+} concentration to 55 mM, the half-activation energy of the Cl^- currents was reduced from 2.20 ± 0.18 (n=8) to 1.68 ± 0.04 (n=10; P=0.012), and the slope factor was increased from –0.233 ± 0.050 (n=8) to –0.112 ± 0.016 (n=10; P=0.026). These results indicate that the CaR stimulation by a rise in the extracellular Ca^{2+} concentration increases volume expansion sensitivity of the swelling-activated Cl^- channel.

DISCUSSION

The present study was undertaken to determine whether the CaR mediates the effects of extracellular Ca^{2+} on the whole-cell volume-sensitive Cl^- current in Intestine 407 cells and, if so, what is the second messenger.

CaR expression in Intestine 407 cells

The G protein-coupled calcium-sensing receptor (CaR) is highly expressed in the parathyroid gland, calcitonin secreting cells of thyroid, and several regions of the kidney where it is involved in regulation of the plasma Ca^{2+} level by modulating secretion of parathyroid hormone or calcitonin and renal tubular Ca^{2+} reabsorption (Brown et al., 1993; 1998). The CaR is known to be also expressed in a wide variety of other tissues that do not have well-established roles in the control of the plasma Ca^{2+} level (Butters et al., 1997; Brown et al., 1998). The CaR has been shown to be expressed in several regions of the gastrointestinal tract (Cima et al., 1997; Gama et al., 1997; Ray et al., 1997; Chattopadhyay et al., 1998; Cheng et al., 1999; Rutten et al., 1999) and in intestinal cell lines, Caco-2 (Kallay et al., 1997) and HT-29 cells (Gama et al., 1997). In the present study, expression of CaR transcripts in another intestinal cell line, Intestine 407, was evidenced by RT-PCR followed by nucleotide sequencing of the amplified products. Sequencing of the PCR product revealed >99% identity with the CaR cloned from human kidney (Aida et al., 1995; Fig. 1). However, there was no difference in amino acid sequence. These results demonstrate that a CaR gene is expressed in Intestine 407 cells. Expression of the CaR protein was verified by

Western analysis which was performed on crude membrane proteins isolated from Intestine 407 cells using an affinity-purified polyclonal antiserum directed against an epitope within extracellular domain of the CaR. Western blotting revealed a major immunoreactive band with molecular mass of around 110 kDa (Fig. 2), which falls in the range (110-205 kDa) of those reported previously in other cell types (Ruat et al., 1995; Bai et al., 1996; Pearce et al., 1996; Quinn et al., 1997; Sands et al., 1997; Chattopadhyay et al., 1998; McNeil et al., 1998; Oda et al., 1998; Rutten et al., 1999).

Upregulation of the VSOR Cl^- channel by CaR

Extracellular Ca^{2+}-induced upregulation of swelling-activated Cl^- currents was first observed in mouse osteoclasts by Sakai et al. (1999). They showed that extracellular Ca^{2+} increases sensitivity of the Cl^- channel to hypotonicity. By simultaneous measurements of cell size and the whole-cell Cl^- current, the present study demonstrated that extracellular Ca^{2+} increases its sensitivity to volume expansion (Fig. 22). The upregulating effect of extracellular Ca^{2+} on the activity of volume-sensitive Cl^- channels in Intestine 407 cells can be deduced to be mediated by activation of G protein-coupled CaR for the following reasons: 1. The cells express the CaR mRNA and protein (Figs. 1 & 2). 2. Extracellular Ca^{2+} augmented whole-cell volume-sensitive Cl^- currents (Fig. 3) with the EC_{50} value (6.5 mM: Fig. 4) which is close to the value reported for the CaR (6.1 mM) of AT-3 prostata cells (Lin et al., 1998). 3. A lesser potent CaR agonist, Mg^{2+}, also enhanced, from the extracellular side, whole-cell volume-sensitive Cl^- currents (Fig. 7), and the EC_{50} value (22.0 mM: Fig. 8) was higher than that for Ca^{2+} and

is close to the value for the CaR of AT-3 prostata cells (23.4 mM: Lin et al., 1998). 4. Other potent CaR agonists, such as La^{3+}, neomycin and spermine, were also found to be effective (Figs. 11, 12 & 13). 5. A G protein inhibitor, GDPβS, abolished the upregulating effect of extracellular Ca^{2+} on the volume-sensitive Cl^- current (Fig. 17). 6. A G protein activator, GTPγS, augmented the swelling-activated Cl^- current (Fig. 15), even under Ca^{2+}- and Mg^{2+}-free conditions, and extracellular Ca^{2+} failed to increase further the VSOR Cl^- current in the presence of GTPγS (Fig. 18).

Second messenger action of cAMP downstream the CaR

The CaR has been reported to control multiple intracellular signaling pathways including IP_3, Ca^{2+}, protein kinase C, cAMP, cGMP, arachidonate, tyrosine kinases and so on (Brown et al., 1993; 1998; Emanuel et al., 1996; Ruat et al., 1996; Tamir et al., 1996; Gama et al., 1997; McNeil et al., 1998). In the present study, I focused only Ca^{2+} and cAMP as the candidates of second messenger. Our preliminary studies with fura-2 showed that intracellular free Ca^{2+} is increased by extracellular Ca^{2+} or another CaR agonist, Gd^{3+} (K. Dezaki, T. Shimizu & Y. Okada, unpublished observations). Therefore, it is possible that the CaR is coupled to Gq in Intestine 407 cells. However, the VSOR Cl^- channel activity is known to be independent of the cytosolic Ca^{2+} level in Intestine 407 cells (Hazama & Okada, 1988). Actually, introduction of BAPTA into the cytosol failed to abolish extracellular Ca^{2+}-induced augmentation of the Cl^- currents (Fig. 20). Even when the cells were preincubated with PTX, extracellular Ca^{2+} augmented the VSOR Cl^- current (Fig. 19). This result may rule out the

involvement of Gi in this signal pathway. After the volume-sensitive Cl^- current was augmented by a rise in intracellular cAMP, extracellular Ca^{2+} could not further enhance the Cl^- current (Fig. 21). Therefore, it is likely that the CaR is coupled to Gs. These results demonstrate that an increase in intracellular cAMP concentration is critically involved in the CaR signal transduction pathway for upregulation of VSOR Cl^- channels in Intestine 407 cells. This line of further investigation may elucidate the mechanism by which osmotic cell swelling activates volume-sensitive Cl^- channel.

Roles of CaR-mediated upregulation of VSOR Cl^- channel

Besides the roles in body Ca^{2+} homeostasis, the CaR has been recently shown to be implicated in a number of fundamental cell functions, such as cell proliferation (Chattopadhyay et al., 1998; Kallay et al., 1997; McNeil et al., 1998; Rutten et al., 1999), apoptosis (Lin et al., 1998) and differentiation (Oda et al., 1998). Via the CaR, extracellular Ca^{2+} has also been reported to regulate several ion channel types, including non-selective Ca^{2+}-permeable cation channels in rat hippocampal neurons (Ye et al., 1996), Ca^{2+}-activated K^+ channels in rat hippocampal neurons (Vassilev et al., 1997) and rat microglial cells (Chattopadhyay et al., 1998; 1999). Here, in Intestine 407 cells, the CaR was, for the first time, shown to mediate extracellular Ca^{2+}-induced upregulation of volume-sensitive Cl^- channels. The present study suggests that the CaR may play an important role in the RVD by upregulating volume-sensitive Cl^- channels. And it is possible that this interaction may transduce, at least in part, the proliferation response, because cell proliferation has been shown to correlate with the cell

volume regulation mechanism (see Okada, 1997; Lang et al., 1998) or extracellular Ca^{2+} (Buras et al., 1995). Furthermore, since the microclimate extracellular Ca^{2+} concentration may increase upon tissue injury or ischemia, there is a possibility that the CaR activation plays a role in cellular defense mechanisms including upregulation of volume-sensitive Cl^- channels in osmotically swollen cells under such pathological conditions. In the intestine, the CaR-mediated mechanism may be implicated in the defense for bacterial infection, because bacteria in the gut produce large amounts of spermine and spermidine (Sarhan et al., 1989; MaCormack & Johnson, 1991).

CaR-independent effects of extracellular divalent cations on VSOR Cl^- current inactivation

Extracellular divalent cations were found to produce an additional effect on whole-cell volume-sensitive Cl^- currents in Intestine 407 cells in the present study. The time course of inactivation observed upon application of large positive potentials became accelerated by extracellular Ca^{2+} (Fig. 5) with the EC_{50} value of 2.5 mM (Fig. 6) or Mg^{2+} (Fig. 9) with the EC_{50} value of 2.1 mM (Fig. 10). These results are in good agreement with previous observations in other cell types (Andersen et al., 1995; Braun and Schulman, 1996; Voets et al., 1997). This apparently blocking effect of Ca^{2+} or Mg^{2+} is not mediated by the CaR, because: 1) both EC_{50} values were quite different from those for the upregulating effect on the Cl^- current amplitude, 2) Mg^{2+} was more potent than Ca^{2+} (Figs. 6 & 10) in contrast to the case of CaR (Figs. 4 & 8), 3) a variety of potent CaR agonists, La^{3+}, neomycin, and spermine, failed to mimic the effect of divalent cations (Figs.

11B, 12B, 13B & 14), and 4) activation of G proteins associated with CaR by GTPγS did not affect the inactivation kinetics of VSOR Cl^- currents at large positive potentials (Fig. 16). Previously, Anderson and coworkers (1995) demonstrated that extracellular Mg^{2+} induces flickering block of the Cl^- channel in outside-out patches from a human small-cell lung cancer cell line (H69AR). However, extracellular Mg^{2+} itself should not act as an open channel blocker, because cationic Mg^{2+} cannot plug into the channel pore from the extracellular side upon application of positive potentials to cells. Thus, it is conceivable that binding of Mg^{2+} to extracellular sites may augment plugging of some impermeant cations from the intracellular side or impermeant anions from the extracellular side. The exact mechanism of the accelerating effect induced by extracellular Ca^{2+} or Mg^{2+} awaits further studies.

ACKNOWLEDGMENTS

I gratefully thank Prof. Y. Okada, my supervisor, for his guidance and support throughout my study. I would like to thank Drs. S. Oiki, S. Morishima, A. Hazama, T. Miyoshi, Y. Akatsuka, K. Dezaki, H-T. Fan and R.Z. Sabirov for helpful discussion throughout this study. Mr. M. Ohara is gratefully acknowledged for technical assistance. I am grateful to all other members of our laboratory for their generous supports.

REFFERENCES

Aida, K., Koishi, S., Tawata, M. & Onaya, T. (1995). Molecular cloning of a putative Ca^{2+}-sensing receptor cDNA from human kidney. *Biochemical and Biophysical Research Communications* **214**, 524-529.

Anderson, J. W., Jirsch, J. D. & Fedida, D. (1995). Cation regulation of anion current activated by cell swelling in two types of human epithelial cancer cells. *Journal of Physiology* **483**, 549-557.

Bai, M., Quinn, S., Trivedi, S., Kifor, O., Pearce, S. H. S., Pollak, M. R., Krapcho, K., Hebert, S. C. & Brown, E. M. (1996). Expression and characterization of inactivating and activating mutations in the human Ca^{2+}_o-sensing receptor. *The Journal of Biological Chemistry* **271**, 19537-19545.

Boynton, A. L. (1988). Calcium and epithelial cell proliferation. *Mineral Electrolyte Metabology* **14**, 86-94.

Braun, A. P. & Schulman, H. (1996). Distinct voltage-dependent gating behaviours of a swelling-activated chloride current in human epithelial cells. *Journal of Physiology* **495**, 743-753.

Brown, E. M. (1991). Extracellular Ca^{2+}-sensing, regulation of parathyroid cell function, and role of Ca^{2+} and other ions as extracellular (first) messengers.

Physiological Reviews **71**, 371-411.

Brown, E. M., Gamba, G., Riccardi, D., Lombardi, M., Butters, R., Kifor, O., Sun, A., Hediger, M. A., Lytton, J. & Hebert, S. C. (1993). Cloning and characterization of an extracellular Ca^{2+}-sensing receptor from bovine parathyroid. *Nature* **366**, 575-580.

Brown, E. M., Pollak, M. & Hebert, S. C. (1998). The extracellular calcium-sensing receptor: its role in health and disease. *Annual Reviews of Medicine* **49**, 15-29.

Buras, R. R., Sabahang, M., Davoodi, F., Schumaker, L. M., Cullen, K. J., Byers, S., Nauta, R. J. & Evans, S. R. T. (1995). The effect of extracellular calcium on colonocytes: evidence for differential responsiveness based upon degree of cell differentiation. *Cell Proliferation* **28**, 245-262.

Butters, R. R. Jr., Chattopadhyay, N., Nielsen, P., Smith, C. P., Mithal, A., Kifor, O., Bai, M., Quinn, S., Goldsmith, P., Hurwitz, S., Krapcho, K., Busby, J. & Brown, E. M. (1997). Cloning and characterization of a calcium-sensing receptor from the hypercalcemic New Zealand white rabbit reveals unaltered responsiveness to extracellular calcium. *Journal of Bone and Mineral Research* **12**, 568-579

Chattopadhyay, N., Ye, C., Yamaguchi, T., Kifor, O., Vassilev, P. M., Nishimura,

R. & Brown, E. M. (1998). Extracellular calcium-sensing receptor in rat oligodendrocytes: Expression and potential role in regulation of cellular proliferation and an outward K^+ channel. *Glia* **24**, 449-458.

Chattopadhyay, N., Ye, C., Yamaguchi, T., Nakai, M., Kifor, O., Vassilev, P. M., Nishimura, R. N. & Brown, E. M. (1999). The extracellular calcium-sensing receptor is expressed in rat microglia and modulates an outward K^+ channel. *Journal of Neurochemistry* **72**, 1915-1922.

Cheng, I., Qureshi, I., Chattopadhyay, N., Qureshi, A., Butters, R. R., Hall, A. E., Cima, R. R., Rogers, K. V., Hebert, S. C., Geibel, J. P., Brown, E. M. & Soybel, D. I. (1999). Expression of an extracellular calcium-sensing receptor in rat stomach. *Gastroenterology* **116**, 118-126.

Cima, R. R., Cheng, I., Klingensmith, M. E., Chattopadhyay, N., Kifor, O., Hebert, S. C., Brown, E. M. & Soybel, D. I. (1997). Identification and functional assay of an extracellular calcium-sensing receptor in *Necturus* gastric mucosa. *American Journal of Physiology* **273**, G1051-G1060.

Emanuel, R. L., Adler, G. K., Kifor, O., Quinn, S. J., Fuller, F., Krapcho, K. & Brown, E. M. (1996). Calcium-sensing receptor expression and regulation by extracellular calcium in the AtT-20 pituitary cell line. *Molecular Endocrinology* **10**, 555-565.

Fan, H-T., Kida, H., Morishima, S., Oiki, S. & Okada, Y. (1999). Effects of phloretin on three types of Cl^- channels in epithelial cells. *The Japanese Journal of Physiology* **49**, Supplement, S109.

Gama, L., Baxendale-cox, L. M. & Breitwieser G. E. (1997). Ca^{2+}-sensing receptors in intestinal epithelium. *American Journal of Physiology* **273**, C1168-C1175.

Giuliano, A. R. & Wood, R. J. (1991). Vitamin D-regulated calcium transport in Caco-2 cells: unique in vitro model. *American Journal of Physiology* **260**, G207-G212.

Hazama, A. & Okada, Y. (1988). Ca^{2+} sensitivity of volume-regulatory K^+ and Cl^- channels in cultured human epithelial cells. *Journal of Physiology* **402**, 687-702.

Hulla, W., Kallay, E., Krugluger, W., Peterlik, M. & Cross, H. S. (1995). Growth control of human colon-adenocarcinoma-derived Caco-2 cells by vitamin-D compounds and extracellular calcium in vitro: relation to c-myc-oncogene and vitamin-D-receptor expression. *International Journal of Cancer* **62**, 711-716.

Kallay, E., Kifor, O., Chattopadhyay, N., Brown, E. M., Bischof, M. G., Peterlik, M. & Cross, H. S. (1997). Calcium-dependent c-*myc* proto-oncogene expression and proliferation of Caco-2 cells: a role for a luminal extracellular

calcium-sensing receptor. *Biochemical and Biophysical Research Communications* **232**, 80-83.

Kubo, M. & Okada, Y. (1992). Volume-regulatory Cl^- channel currents in cultured human epithelial cells. *Journal of Physiology* **456**, 351-371.

Lang, F. (1998). Cell Volume Regulation. Karger, Basel. 264pp.

Lang, F., Busch, G. L., Ritter, M., Volkl, H., Waldegger, S., Gulbins, E. & Haussinger, D. (1998). Functional significance of cell volume regulatory mechanisms. *Physiological Reviews* **78**, 247-306.

Lin, K., Chattopadhyay, N., Bai, M., Alvarez, R., Dang, C. V., Baraban, J. M., Brown, E. M. & Ratan, R. R. (1998). Elevated extracellular calcium can prevent apoptosis via the calcium-sensing receptor. *Biochemical and Biophysical Research Communications* **249**, 325-331.

Liu, Y., Oiki, S., Tsumura, T., Shimizu, T. & Okada, Y. (1998). Glibenclamide blocks volume-sensitive Cl^- channels by dual mechanisms. *American Journal of Physiology* **275**, C343-C351.

MaCormack, S. A., & Johnson, L. R. (1991). Role of polyamines in gastrointestinal mucosal growth. *American Journal of Physiology* **260**, G795-G806.

McNeil, S. E., Hobson, S. A., Nipper, V. & Rodland, K. D. (1998). Functional calcium-sensing receptors in rat fibroblasts are required for activation of SRC kinase and mitogen-activated protein kinase in response to extracellular calcium. *The Journal of Biological Chemistry* **273**, 1114-1120.

Miwa, A., Ueda, K. & Okada, Y. (1997). Protein kinase C-independent correlation between P-glycoprotein expression and volume sensitivity of Cl^- channel. *The Journal of Membrane Biology* **157**, 63-69.

Nemeth, E. F. (1998). Cell physiology source book: Regulation of Cellular Functions by Extracellular Calcium. Academic Press, California, 142-152.

Nilius, B., Eggermont, J., Voets, T., Buyse, G., Manolopoulos, V. & Droogmans, G. (1997). Properties of volume-regulated anion channels in mammalian cells. *Progress in Biophysics and Molecular Biology* **68**, 69-119.

Oda, Y., Tu, C.-L., Pillai, S. & Bikle, D. D. (1998). The calcium sensing receptor and its alternatively spliced form in keratinocyte differentiation. *The Journal of Biological Chemistry* **273**, 23344-23352.

Okada, Y. (1997). Volume expansion-sensing outward-rectifier Cl^- channel: fresh start to the molecular identity and volume sensor. *American Journal of Physiology* **273**, C755-C789.

Okada, Y. (1998). Cell Volume Regulation: The Molecular Mechanism and Volume Sensing Machinery. Elsevier, Amsterdam. 214pp.

Okada, Y., Oiki, S., Hazama, A. & Morishima, S. (1998). Criteria for the molecular identification of the volume-sensitive outwardly rectifying Cl^- channel. *The Journal of General Physiology* **112**, 365-367.

Pearce, S. H. S., Bai, M., Quinn, S. J., Kifor, O., Brown, E. M. & Thakker, R. V. (1996). Functional characterization of calcium-sensing receptor mutations expressed in human embryonic kidney cells. *Journal of Clinical Investigation* **98**, 1860-1866.

Quinn, S. J., Ye, C., Diaz, R., Kifor, O., Bai, M., Vassilev, P. & Brown, E. M. (1997). The Ca^{2+}-sensing receptor: a target for polyamines. *American Journal of Physiology* **273**, C1315-C1323.

Ray, J. M., Squires, P. E., Curtis, S. B., Meloche, M. R. & Buchan, A. M. (1997). Expression of the calcium-sensing receptor on human antral gastrin cells in culture. *Journal of Clinical Investigation* **99**, 2328-2333.

Ruat, M., Molliver, M. E., Snowman, A. M. & Snyder, S. H. (1995). Calcium sensing receptor: Molecular cloning in rat and localization to nerve terminals. *Proceedings of the National Academy of Sciences of the United States of*

America **92**, 3161-3165.

Ruat, M., Snowman, A. M., Hester, L. D. & Snyder, S. H. (1996). Cloned and expressed rat Ca^{2+}-sensing receptor. *The Journal of Biological Chemistry* **271**, 5972-5975.

Rutten, M. J., Bacon, K. D., Marlink, K. L., Stoney, M., Meichsner, C. L., Lee, F. P., Hobson, S. A., Rodland, K. D., Sheppard, B. C., Trunkey, D. D., Deveney, K. E. & Deveney, C. W. (1999). Identification of a functional Ca^{2+}-sensing receptor in normal human gastric mucous epithelial cells. *American Journal of Physiology* **277**, G662-G670.

Sakai, H., Nakamura, F. & Kuno, M. (1999) Synergetic activation of outwardly rectifying Cl^- currents by hypotonic stress and external Ca^{2+} in murine osteoclasts. *Journal of Physiology* **515**, 157-168.

Sands, J. M., Naruse, M., Baum, M., Jo, I., Hebert, S. C., Brown, E. M. & Harris, H. W. (1997). Apical extracellular calcium/polyvalent cation-sensing receptor regulates vasopressin-elicited water permeability in rat kidney inner medullary collecting duct. *Journal of Clinical Investigation* **99**, 1399-1405.

Sarhan, S., Knodgen, B. & Seiler, N. (1989). The gastrointestinal tract as polyamine source for tumor growth. *Anticancer Research* **9**, 215-223.

Shimizu, T., Morishima, S., Kida, H. & Okada, Y. (1999). Volume-sensitivity of swelling-activated chloride currents in human Intestine 407 cells: Possible relation to the spring energy of cytoskeleton. *The FASEB Journal* **13**, A712 (Abstract).

Strange, K., Emma, F. & Jackson, P. S. (1996).Cellular and molecular physiology of volume-sensitive anion channels. *American Journal of Physiology* **270**, C711-C730..

Tamir, H., Liu, K., Adlersberg, M., Hsiung, S. & Gershon, M. D. (1996). Acidification of serotonin-containing secretory vesicles induced by a plasma membrane calcium receptor. *The Journal of Biological Chemistry* **271**, 6441-6450.

Tsumura, T., Oiki, S., Ueda, S., Okuma, M. & Okada, Y. (1996). Sensitivity of volume-sensitive Cl^- conductance in human epithelial cells to extracellular nucleotides. *American Journal of Physiology* **271**, C1872-C1878.

Vassilev, P. M., Ho-Pao, C. L., Knazirska, M. P. V., Ye, C., Hong, K., Seidman, C. E., Seidman, J. G. & Brown, E. M. (1997). Ca_o-sensing receptor (CaR)-mediated activation of K^+ channels is blunted in CaR gene-deficient mouse neurons. *NeuroReport* **8**, 1411-1416.

Voets, T., Droogmans, G. & Nilius, B. (1997). Modulation of voltage-dependent

properties of a swelling-activated Cl^- current. *The Journal of General Physiology* **110**, 313-325.

Worrell, R. T., Butt, A. G., Cliff, W. H. & Frizzell, R. A. (1989). A volume-sensitive chloride conductance in human colonic cell line T84. *American Journal of Physiology* **256**, C1111-C1119.

Ye, C., kanazirska, M., Quinn, S., Brown, E. M.. & Vassilev, P. M. (1996). Modulation by polycationic Ca^{2+}-sensing receptor agonists of nonselective cation channels in rat hippocampal neurons. *Biochemical and Biophysical Research Communications* **224**, 271-280.

Figure Legends

Figure 1. Expression of the CaR mRNA assessed by RT-PCR analysis in Intestine 407 cells.

A) Gel analysis of the CaR-specific PCR product (predicted to be 340 bp) from Intestine 407 cells. *Lane 1*: marker (100 bp DNA ladder), *lane 2*: PCR product with reverse transcriptase, and *lane 3*: negative control without reverse transcriptase. *B*) Nucleotide sequence of a subcloned RT-PCR product from Intestine 407 cells (designated as I407CaR) aligned with the sequence of the human kidney CaR (HuKCaSR) cDNA clone. Difference between HuKCaSR and I407CaR is designated by *asterisk*.

Figure 2. Expression of the CaR protein by Western analysis in Intestine 407 cells.

Western blot analysis was performed on 30 μg of crude plasma membrane proteins from Intestine 407 cells using an affinity-purified polyclonal anti-rat CaR antibody (*lane 1*), as described in *Materials and Methods*. *Lane 2* is the negative control. Molecular mass is shown at *left*.

Figure 3. Effects of extracellular Ca^{2+} on whole-cell volume-sensitive Cl^- current.

A) Representative record before and after exposure to hypotonic solution in the absence or presence of extracellular 10 mM Ca^{2+} during application of alternating 2-s pulses (0 to ±40 mV) or of step pulses from −100 mV to +100 mV

in 20-mV increments (at *asterisks*). Gain of chart recorder was changed by one-half at 2nd and 3rd *asterisks*. *B*) Expanded traces of current responses (*a* & *b* in *A*) to step pulses (protocol shown in *Inset*) in the absence (*a*) and presence (*b*) of Ca^{2+}. *Arrowheads*, zero-current level. *C*) Current-voltage relationships in the absence (*filled circles*) and presence (*open circles*) of Ca^{2+}. Each point represents the mean instantaneous current of 5 observations with S.E.M. Differences between values with and without Ca^{2+} at each potential are statistically significant (P=0.006–0.012).

Figure 4. Concentration dependency of extracellular Ca^{2+} effect on the VSOR Cl^- current.

Whole-cell instantaneous currents were recorded at –40 mV, and the relative current densities were calculated by dividing the values in the presence of Ca^{2+} by those measured in the absence of Ca^{2+} and plotted against the extracellular Ca^{2+} concentration (means ± S.E.M. of 3–9 observations). The EC_{50} was 6.5 mM.

Figure 5. Effects of extracellular Ca^{2+} on depolarization-induced inactivation of the VSOR Cl^- current.

A) Inactivation time courses during application of steps to +120 mV in the absence and presence of extracellular 55 mM Ca^{2+}. Smooth curves are biexponential fits. *B*) Fast time constants (τ_f) in the absence (*filled circles*) and presence (*open circles*) of extracellular Ca^{2+}. *C*) Slow time constants (τ_s). Each symbol in *B* and *C* represents the mean ± S.E.M. (n=4–9). Differences between values with and without Ca^{2+} at each potential are statistically significant

(P=0.003–0.027) except for τ_f values at 80 mV (P=0.054).

Figure 6. Concentration dependency of extracellular Ca^{2+} effect on the half inactivation time of VSOR Cl^- currents.

The half inactivation time was evaluated from the VSOR Cl^- current recorded at +100 mV. The relative half inactivation time was calculated by dividing the value in the presence of Ca^{2+} by that measured in the absence of Ca^{2+} and plotted against the extracellular Ca^{2+} concentration (means ± S.E.M. of 3–6 observations). The maximum inhibition was 60.4%, and the EC_{50} 2.5 mM.

Figure 7. Effects of extracellular Mg^{2+} on the VSOR Cl^- current.

A) Representative record before and after exposure to hypotonic solution in the absence or presence of extracellular 20 mM Mg^{2+} during application of alternating 2-s pulses (0 to ±40 mV) or of step pulses from −100 mV to +100 mV in 20-mV increments (at *asterisks*). Gain of chart recorder was changed by one-half at 2nd and 3rd *asterisks*. *B*) Expanded traces of current responses (*a* & *b* in *A*) to step pulses in the absence (*a*) and presence (*b*) of Mg^{2+}. *Arrowheads*, zero-current level. *C*) Current-voltage relationships in the absence (*filled circles*) and presence (*open circles*) of Mg^{2+}. Each point represents the mean instantaneous current of 13 observations with S.E.M. Differences between values with and without Mg^{2+} at each potential are statistically significant (P=0.023–0.049) except at 0 mV (P=0.149).

Figure 8. Concentration dependency of extracellular Mg^{2+} effect on the VSOR Cl^- current.

Whole-cell instantaneous currents were recorded at −40 mV, and the relative current densities were calculated by dividing the values in the presence of Mg^{2+} by those measured in the absence of Mg^{2+} and plotted against the extracellular Mg^{2+} concentration (means ± S.E.M. of 3–13 observations). The EC_{50} was 22.0 mM.

Figure 9. Effects of extracellular Mg^{2+} on depolarization-induced inactivation of the VSOR Cl^- current.

A) Inactivation time courses during application of steps to +120 mV in the absence and presence of extracellular 55 mM Mg^{2+}. Smooth curves are biexponential fits. *B*) Fast time constants (τ_f) in the absence (*filled circles*) and presence (*open circles*) of extracellular Ca^{2+}. *C*) Slow time constants (τ_s). Each symbol in *B* and *C* represents the mean ± S.E.M. (n=4–10). Differences between values with and without Ca^{2+} at each potential are statistically significant (P=0.009–0.041).

Figure 10. Concentration dependency of extracellular Mg^{2+} effect on the half inactivation time of VSOR Cl^- currents.

The half inactivation time was evaluated from the VSOR Cl^- current recorded at +100 mV. The relative half inactivation time was calculated by dividing the value in the presence of Mg^{2+} by that measured in the absence of Mg^{2+} and plotted against the extracellular Mg^{2+} concentration (means ± S.E.M. of 3–11

observations). The maximum inhibition was 40.7%, and the EC_{50} 2.1 mM.

Figure 11. Effects of extracellular La^{3+} on the VSOR Cl^- current.

A) Representative record before and after exposure to hypotonic solution in the absence or presence of extracellular 3 μM La^{3+} during application of alternating 2-s pulses (0 to ±40 mV) or of step pulses from −100 mV to +100 mV in 20-mV increments (at *asterisks*). Gain of chart recorder was changed by one-half at *asterisks*. *B*) Expanded traces of current responses (*a* & *b* in *A*) to step pulses in the absence (*a*) and presence (*b*) of La^{3+}. *Arrowheads*, zero-current level. *C*) Current-voltage relationships in the absence (*filled circles*) and presence (*open circles*) of La^{3+}. Each point represents the mean instantaneous current of 5 observations with S.E.M. Differences between values with and without La^{3+} at each potential are statistically significant (P=0.029–0.038) except at 0 mV (P=0.061).

Figure 12. Effects of neomycin on the VSOR Cl^- current.

A) Representative record before and after exposure to hypotonic solution in the absence or presence of extracellular 500 μM neomycin during application of alternating 2-s pulses (0 to ±40 mV) or of step pulses from −100 mV to +100 mV in 20-mV increments (at *asterisks*). Gain of chart recorder was changed by one-half at 2nd and 3rd *asterisks*. *B*) Expanded traces of current responses (*a* & *b* in *A*) to step pulses in the absence (*a*) and presence (*b*) of neomycin. *Arrowheads*, zero-current level. *C*) Current-voltage relationships in the absence (*filled circles*) and presence (*open circles*) of neomycin. Each point represents the mean

instantaneous current of 7 observations with S.E.M. Differences between values with and without neomycin at each potential are statistically significant (P=0.006–0.016) except at 0 mV (P=0.120).

Figure 13. Effects of spermine on the VSOR Cl^- current.

A) Representative record before and after exposure to hypotonic solution in the absence or presence of extracellular 1 mM spermine during application of alternating 2-s pulses (0 to ±40 mV) or of step pulses from −100 mV to +100 mV in 20-mV increments (at *asterisks*). *B*) Expanded traces of current responses (*a* & *b* in *A*) to step pulses in the absence (*a*) and presence (*b*) of spermine. *Arrowheads*, zero-current level. *C*) Current-voltage relationships in the absence (*filled circles*) and presence (*open circles*) of spermine. Each point represents the mean instantaneous current of 9 observations with S.E.M. Differences between values with and without spermine at each potential are statistically significant (P=0.016–0.047).

Figure 14. Effects of neomycin on depolarization-induced inactivation of the VSOR Cl^- current.

The inactivation time constants at +100 mV in the absence (*filled columns*, n=4) and presence (*open columns*, n=3) of 500 μM neomycin. *Left*, fast time constants (τ_f). *Right*, slow time constants (τ_s). Each column represents the mean ± S.E.M. Differences between values with and without neomycin are not statistically significant (τ_f, P=0.331; τ_s, P=0.247).

Figure 15. Effects of GDPβS and GTPγS on the instantaneous VSOR Cl^- current under Ca^{2+}- and Mg^{2+}-free conditions.

A) Representative record before and after exposure to Ca^{2+}- and Mg^{2+}-free hypotonic solution in the presence of intracellular 500 μM GDPβS (*left*) or GTPγS (*right*) during application of alternating 2-s pulses (0 to ±40 mV) or of step pulses from −100 mV to +100 mV in 20-mV increments (at *asterisks*). Gain of chart recorder was changed by one-half at *asterisks* except for 1st *asterisk* in the presence of GDPβS. *B*) Expanded traces of current responses (*a* & *b* in *A*) to step pulses in the presence of GDPβS (*a*) or GTPγS (*b*). *Arrowheads*, zero-current level. C) Current-voltage relationships in the absence (*filled circles*, n=14) and presence of intracellular 500 μM GDPβS (*open circles*, n=7) or 500 μM GTPγS (*open triangles*, n=7). Each point represents the mean ± S.E.M. Differences between values with and without GTPγS at each potential are statistically significant (P=0.011–0.050) except at 0 mV (P=0.390), but not between those with and without GDPβS (P=0.086–0.314).

Figure 16. Effects of GDPβS and GTPγS on depolarization-induced inactivation of the VSOR Cl^- current.

The inactivation time constants at +100 mV in the absence (*filled columns*, n=13) and presence of intracellular 500 μM GDPβS (*open columns*, n=5) or 500 μM GTPγS (*hatched columns*, n=4). *Left*, fast time constants (τ_f) *Right*, slow time constants (τ_s). Each column represents the mean ± S.E.M. Differences between values with and without GDPβS or GTPγS are not statistically significant (τ_f, GDPβS: P=0.344, GTPγS: P=0.405; τ_s, GDPβS: P=0.386, GTPγS: P=0.337).

Figure 17. Effects of GDPβS on the Ca^{2+}-induced change in VSOR Cl^- currents.

A) Representative record before and after exposure to hypotonic solution in the absence or presence of extracellular 10 mM Ca^{2+} during application of alternating 2-s pulses (0 to ±40 mV) or of step pulses from −100 mV to +100 mV in 20-mV increments (at *asterisks*). GDPβS (500 μM) was added to pipette (intracellular) solution. Gain of chart recorder was changed by one-half at 2nd and 3rd *asterisks*. *B*) Expanded traces of current responses (*a* & *b* in *A*) to step pulses in the absence (*a*) and presence (*b*) of Ca^{2+} with GDPβS. *Arrowheads*, zero-current level. *C*) Current-voltage relationships in the absence (*filled circles*) and presence (*open circles*) of Ca^{2+} with added GDPβS to pipette solution. Each point represents the mean instantaneous current of 7 observations with S.E.M. Differences between values with and without Ca^{2+} at each potential are not statistically significant (P=0.186–0.327).

Figure 18. Effects of GTPγS on the Ca^{2+}-induced change in VSOR Cl^- currents.

A) Representative record before and after exposure to hypotonic solution in the absence or presence of extracellular 10 mM Ca^{2+} during application of alternating 2-s pulses (0 to ±40 mV) or of step pulses from −100 mV to +100 mV in 20-mV increments (at *asterisks*). GTPγS (500 μM) was added to pipette solution. Gain of chart recorder was changed by one-half at *asterisks*. *B*) Expanded traces of current responses (*a* & *b* in *A*) to step pulses in the absence (*a*) and presence (*b*) of Ca^{2+} with GTPγS. *Arrowheads*, zero-current level. *C*)

Current-voltage relationships in the absence (*filled circles*) and presence (*open circles*) of Ca^{2+} with added GTPγS to pipette solution. Each point represents the mean instantaneous current of 7 observations with S.E.M. Differences between values with and without Ca^{2+} at each potential are not statistically significant (P=0.326–0.439).

Figure 19. Effects of PTX on the Ca^{2+}-induced change in VSOR Cl^- currents.

A) Representative record before and after exposure to hypotonic solution in the absence or presence of extracellular 10 mM Ca^{2+} during application of alternating 2-s pulses (0 to ±40 mV) or of step pulses from −100 mV to +100 mV in 20-mV increments (at *asterisks*). Cells were preincubated for 24 h with 100 ng/ml PTX, and PTX was also added to pipette solution. Gain of chart recorder was changed by one-half at *asterisks*. *B*) Expanded traces of current responses (*a* & *b* in *A*) to step pulses in the absence (*a*) and presence (*b*) of Ca^{2+} with PTX. *Arrowheads*, zero-current level. *C*) Current-voltage relationships in the absence (*filled circles*) and presence (*open circles*) of Ca^{2+} with added PTX to pipette solution. Each point represents the mean instantaneous current of 4 observations with S.E.M. Differences between values with and without Ca^{2+} at each potential are statistically significant (P=0.006–0.041) except at 0 mV (P=0.151).

Figure 20. Effects of BAPTA on the Ca^{2+}-induced change in VSOR Cl^- currents.

A) Representative record before and after exposure to hypotonic solution in the absence or presence of extracellular 10 mM Ca^{2+} during application of

alternating 2-s pulses (0 to ±40 mV) or of step pulses from −100 mV to +100 mV in 20-mV increments (at *asterisks*). BAPTA (5 mM) was added to pipette solution. Gain of chart recorder was changed by one-half at 2nd and 3rd *asterisks*. *B*) Expanded traces of current responses (*a* & *b* in *A*) to step pulses in the absence (*a*) and presence (*b*) of Ca^{2+} with BAPTA. *Arrowheads*, zero-current level. *C*) Current-voltage relationships in the absence (*filled circles*) and presence (*open circles*) of Ca^{2+} with added BAPTA to pipette solution. Each point represents the mean instantaneous current of 5 observations with S.E.M. Differences between values with and without Ca^{2+} at each potential are statistically significant (P=0.022–0.043).

Figure 21. Effects of intracellular cAMP on the Ca^{2+}-induced change in VSOR Cl^- currents.

A) Representative record before and after exposure to Ca^{2+}-free or 10 mM Ca^{2+} hypotonic solution in the absence or presence of extracellular cocktail during application of alternating 2-s pulses (0 to ±40 mV) or of step pulses from −100 mV to +100 mV in 20-mV increments (at *asterisks*). The cocktail contained forskolin (10 μM), dibutylyl cAMP (1 mM) and IBMX (400 μM). Gain of chart recorder was changed by one-half at 2nd, 3rd, and 4th *asterisks*. *B*) Expanded traces of current responses to step pulses (*a* & *b* in *A*). *Arrowheads*, zero-current level. *C*) Current-voltage relationships of volume-sensitive Cl^- currents before (*filled circles*) and after cAMP stimulation in the absence (*open circles*) and presence of Ca^{2+} (*open triangles*). Each point represents the mean instantaneous current of 4 observations with S.E.M. Differences between values with and without cocktail

at each potential are statistically significant under Ca^{2+}-free conditions (P=0.003–0.017), but those between Ca^{2+}-free and 10 mM Ca^{2+} conditions during cAMP stimulation are not significant (P=0.072–0.438).

Figure 22. Volume expansion sensitivity of swelling-activated Cl^- currents

Relationships between two parameters simultaneously recorded: whole-cell Cl^- current density and relative outer surface area of simple spherical morphology. *Filled circles* and *open circles* indicate the current densities in the absence and presence of extracellular Ca^{2+} (55 mM), respectively. A) All the data collected in the absence (n=8) and presence (n=10) of Ca^{2+}. B) Representative data fitted to Boltzmann function in the absence and presence of Ca^{2+}. The half activation energy was reduced from 2.20 to 1.68 and the slope factor increased from −0.23 to −0.11 by an increase in extracellular Ca^{2+}.

A

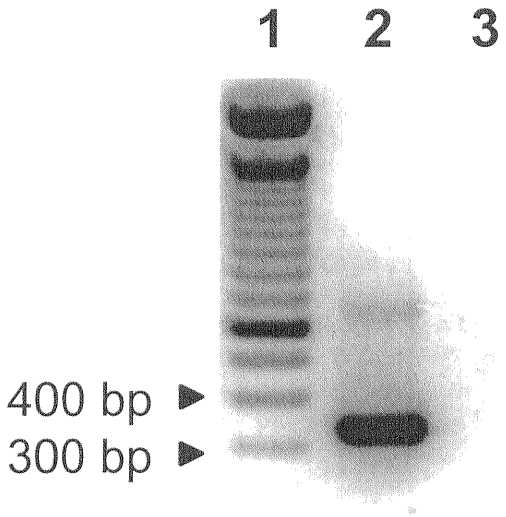

B

HuKCaSR	CACAATTGCA	GCTGATGACG	ACTATGGGCG	GCCGGGGATT	GAGAAATTCC	707
I407CaR	CACAATTGCA	GCTGATGACG	ACTATGGGCG	GCCGGGGATT	GAGAAATTCC	50
HuKCaSR	GAGAGGAAGC	TGAGGAAAGG	GATATCTGCA	TCGACTTCAG	TGAACTCATC	757
I407CaR	GAGAGGAAGC	TGAGGAAAGG	GATATCTGCA	TCGACTTCAG	TGAACTCATC	100
			*			
HuKCaSR	TCCCAGTACT	CTGATGAGGA	GGAGATCCAG	CATGTGGTAG	AGGTGATTCA	807
I407CaR	TCCCAGTACT	CTGATGAGGA	AGAGATCCAG	CATGTGGTAG	AGGTGATTCA	150
HuKCaSR	AAATTCCACG	GCCAAAGTCA	TCGTGGTTTT	CTCCAGTGGC	CCAGATCTTG	857
I407CaR	AAATTCCACG	GCCAAAGTCA	TCGTGGTTTT	CTCCAGTGGC	CCAGATCTTG	200
HuKCaSR	AGCCCCTCAT	CAAGGAGATT	GTCCGGCGCA	ATATCACGGG	CAAGATCTGG	907
I407CaR	AGCCCCTCAT	CAAGGAGATT	GTCCGGCGCA	ATATCACGGG	CAAGATCTGG	250
HuKCaSR	CTGGCCAGCG	AGGCCTGGGC	CAGCTCCTCC	CTGATCGCCA	TGCCTCAGTA	957
I407CaR	CTGGCCAGCG	AGGCCTGGGC	CAGCTCCTCC	CTGATCGCCA	TGCCTCAGTA	300
HuKCaSR	CTTCCACGTG	GTTGGCGGCA	CCATTGGATT	CGCTCTGAAG		997
I407CaR	CTTCCACGTG	GTTGGCGGCA	CCATTGGATT	CGCTCTGAAG		340

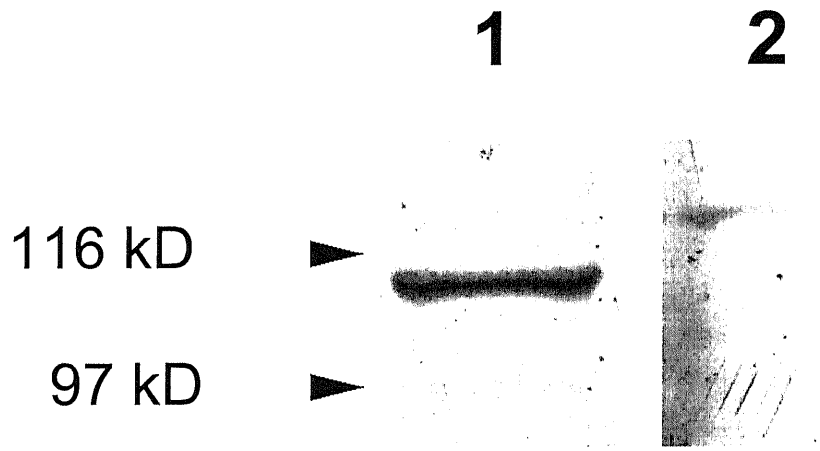
1
2
116 kD
97 kD

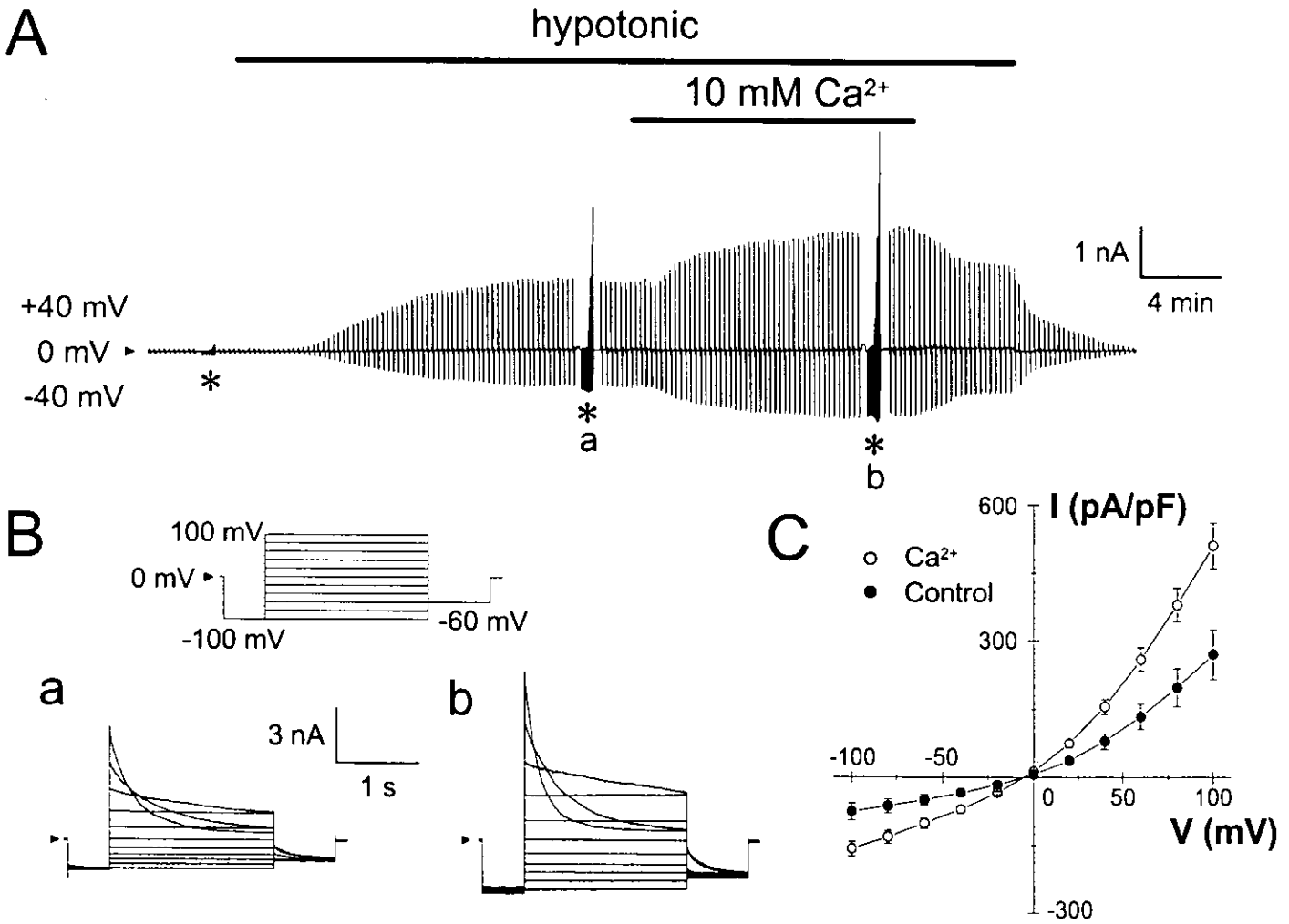
A
hypotonic
10 mM Ca2+
1 nA
4 min
+40 mV
0 mV
-40 mV
a
b
B
100 mV
0 mV
-60 mV
-100 mV
a
3 nA
1 s
b
C
I (pA/pF)
600
300
-300
Ca2+
Control
-100
-50
0
50
100
V (mV)

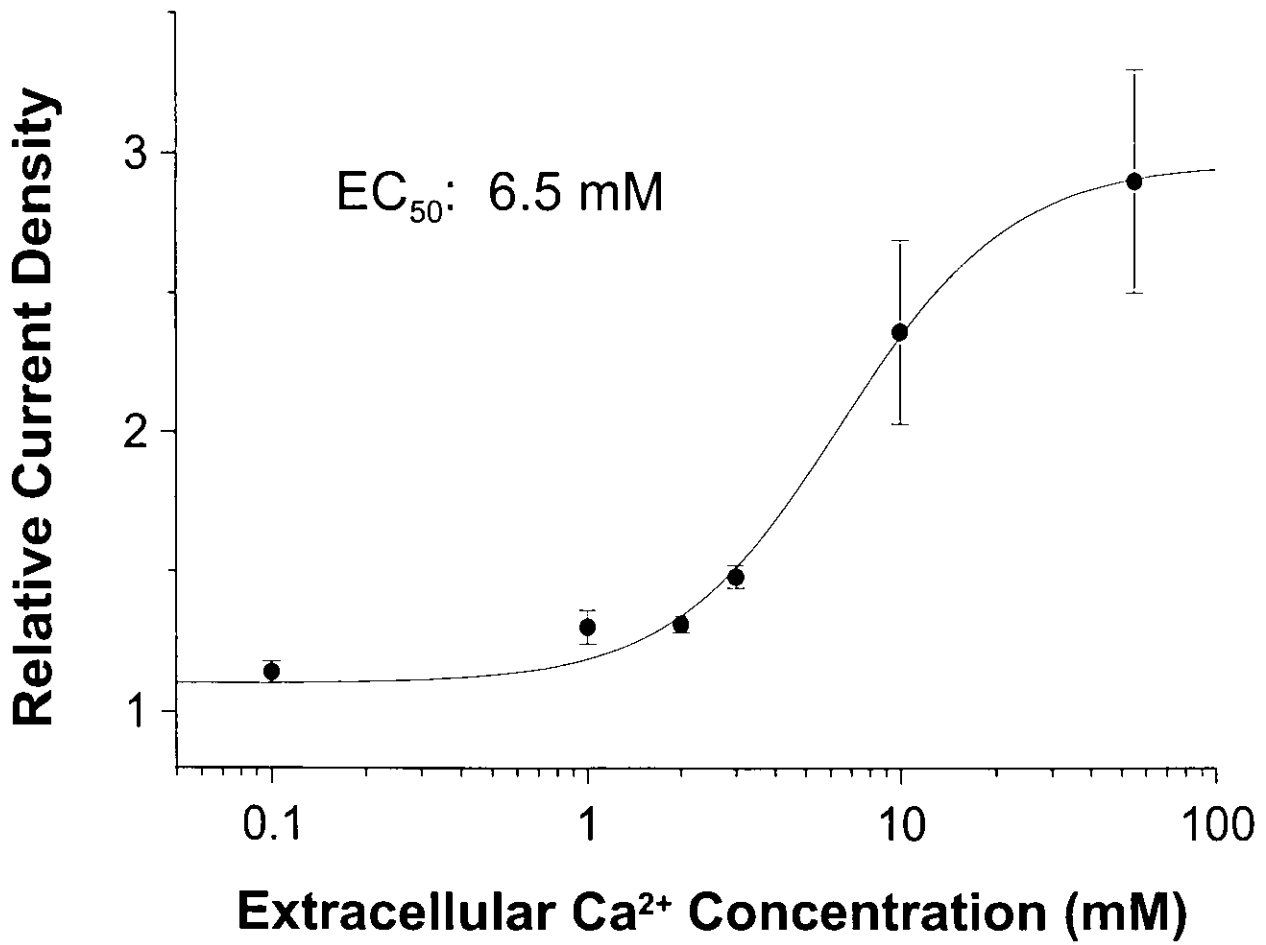
Relative Current Density
3
2
1
EC50: 6.5 mM
0.1
1
10
100
Extracellular Ca2+ Concentration (mM)

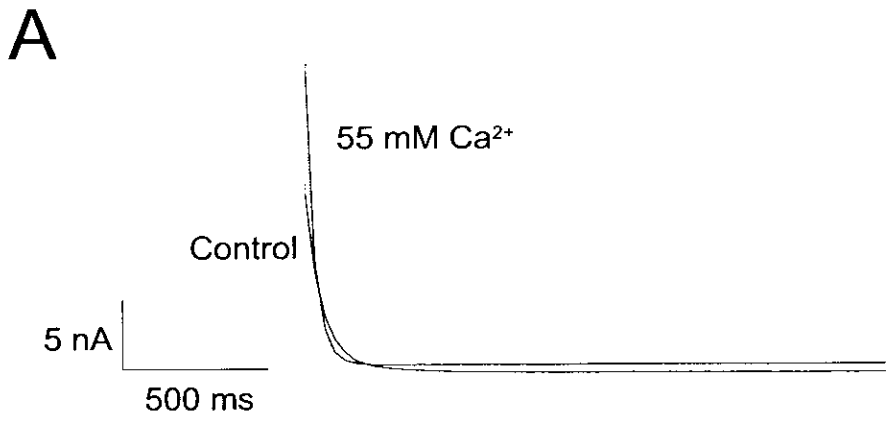
A
55 mM Ca2+
Control
5 nA
500 ms

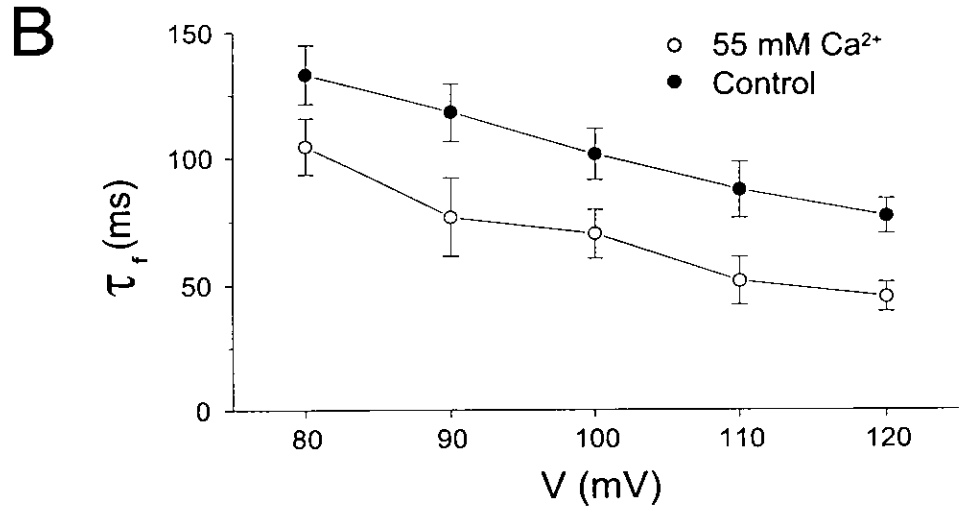
B
150
100
50
0
τf (ms)
55 mM Ca2+
Control
80
90
100
110
120
V (mV)

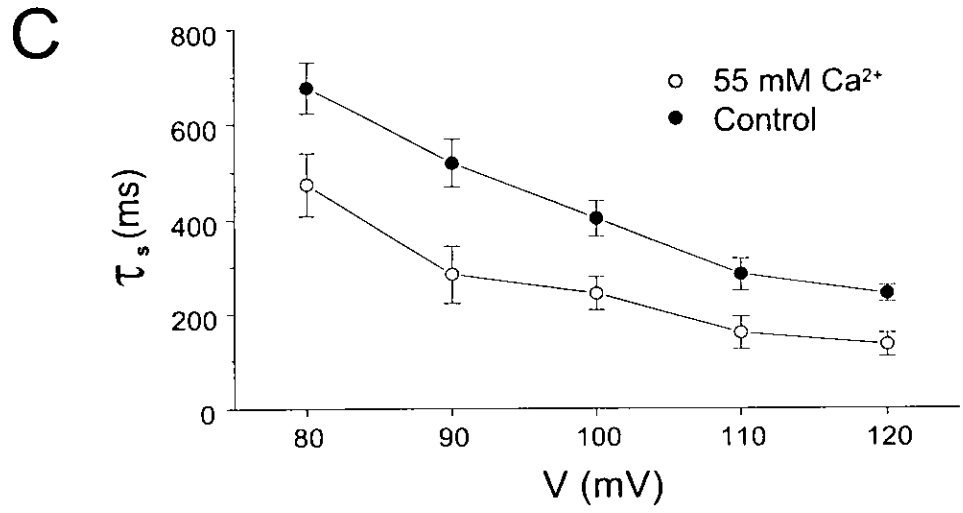
C
800
600
400
200
0
τs (ms)
55 mM Ca2+
Control
80
90
100
110
120
V (mV)

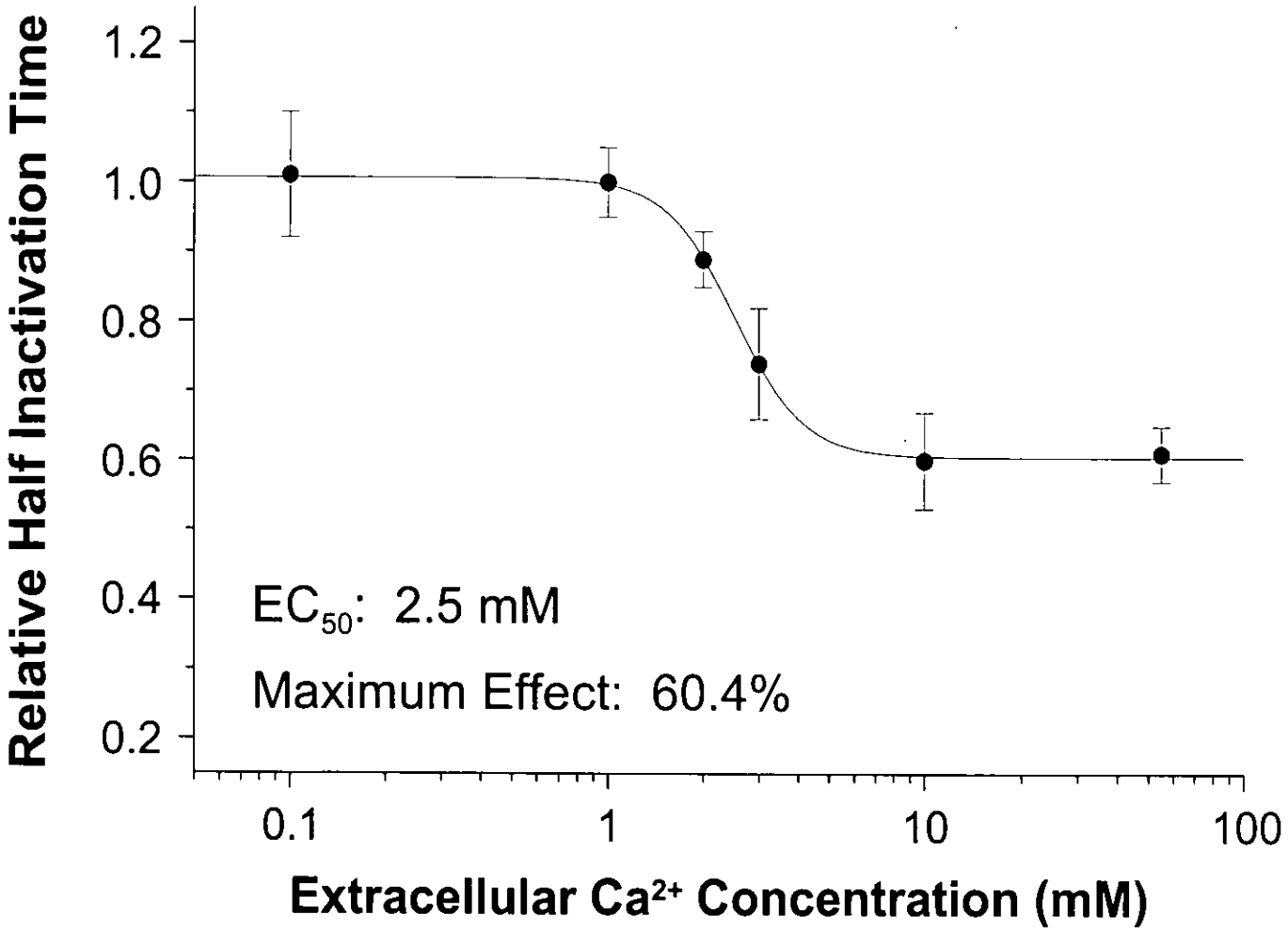
Relative Half Inactivation Time
1.2
1.0
0.8
0.6
0.4
0.2
EC50: 2.5 mM
Maximum Effect: 60.4%
0.1
1
10
100
Extracellular Ca2+ Concentration (mM)

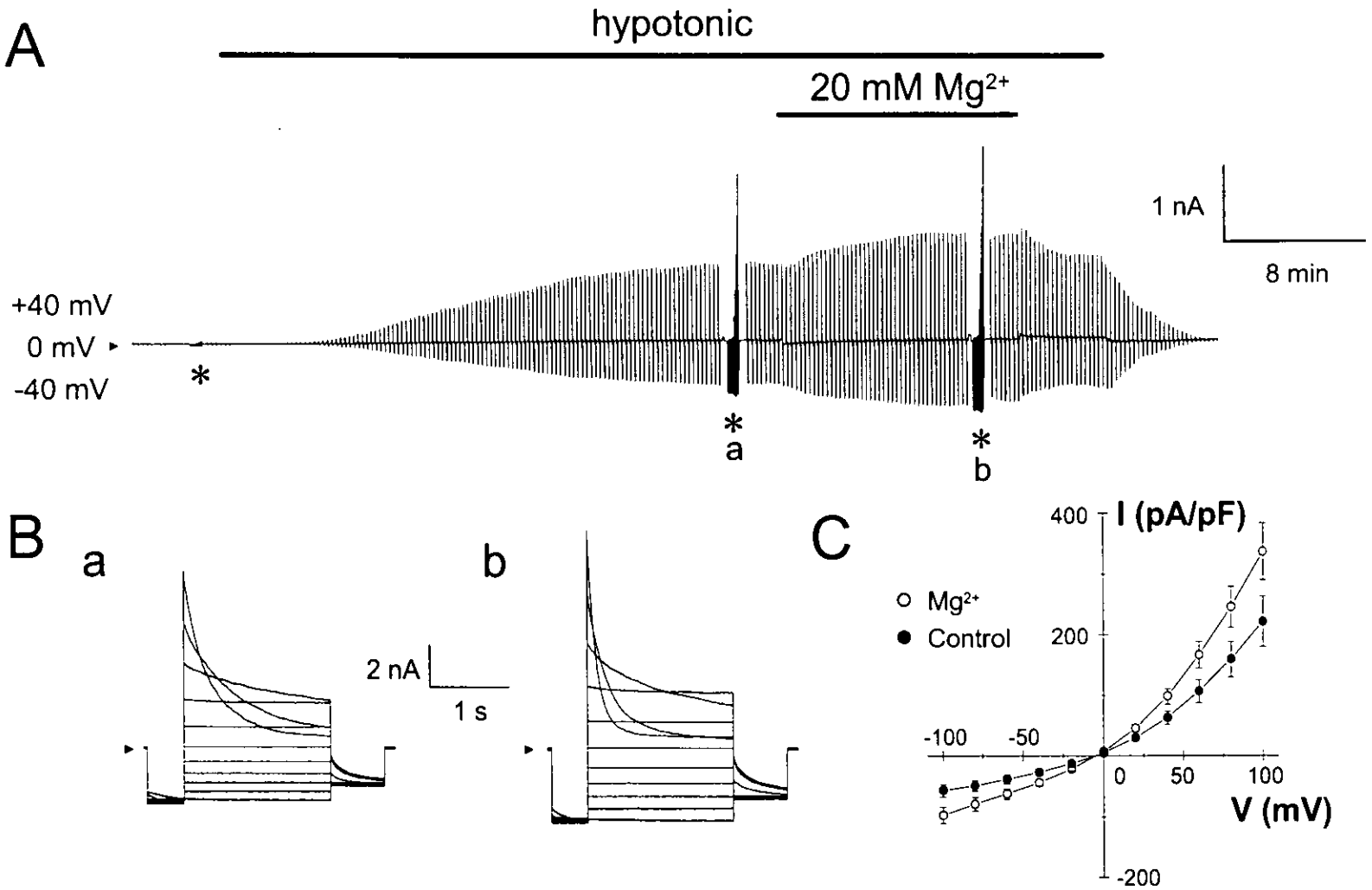
A
hypotonic
20 mM Mg2+
1 nA
8 min
+40 mV
0 mV
-40 mV
*
*
a
*
b
B
a
b
2 nA
1 s
C
400
I (pA/pF)
Mg2+
Control
200
-100
-50
0
50
100
V (mV)
-200

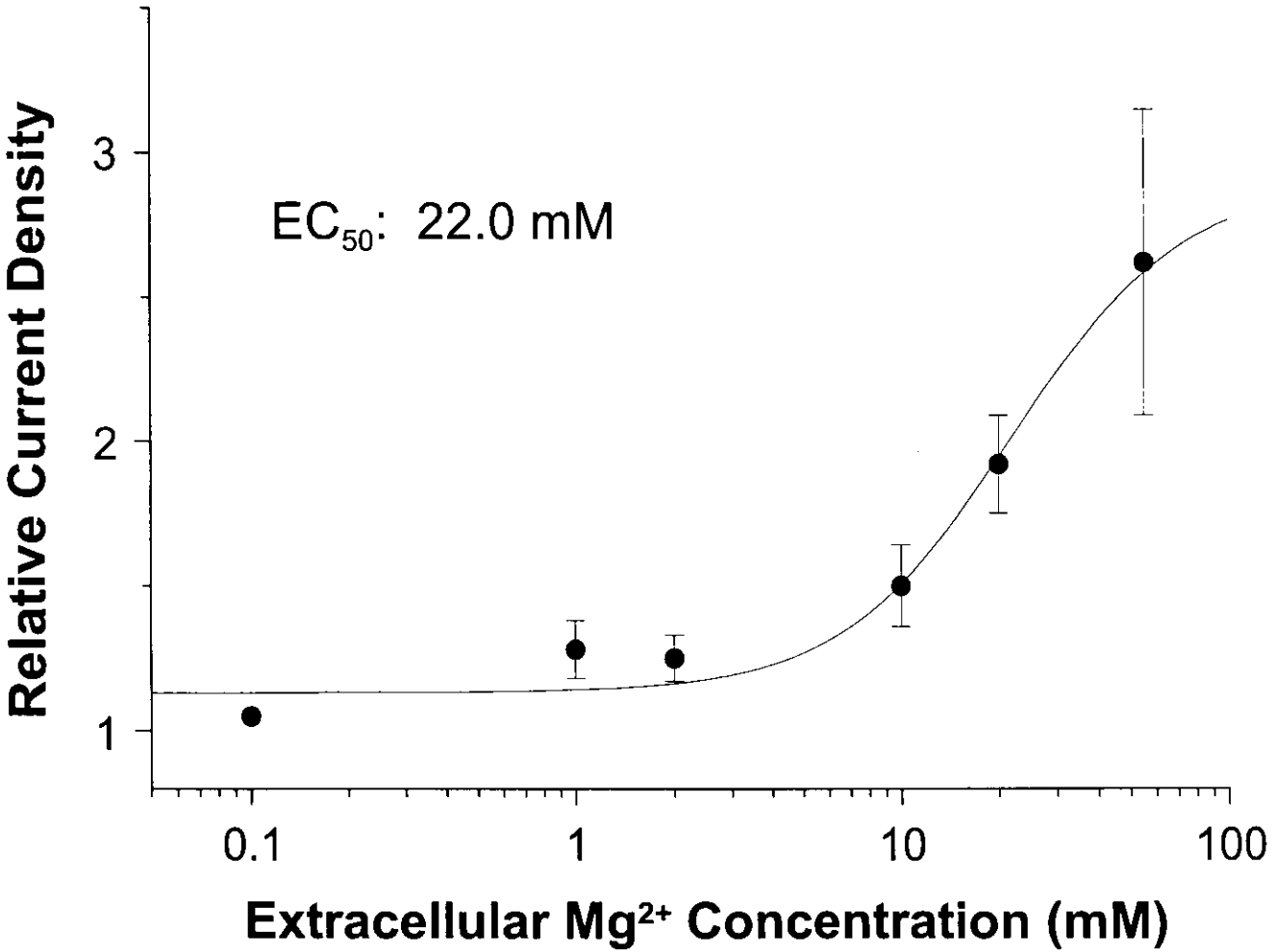
Relative Current Density
3
2
1
EC50: 22.0 mM
0.1
1
10
100
Extracellular Mg2+ Concentration (mM)

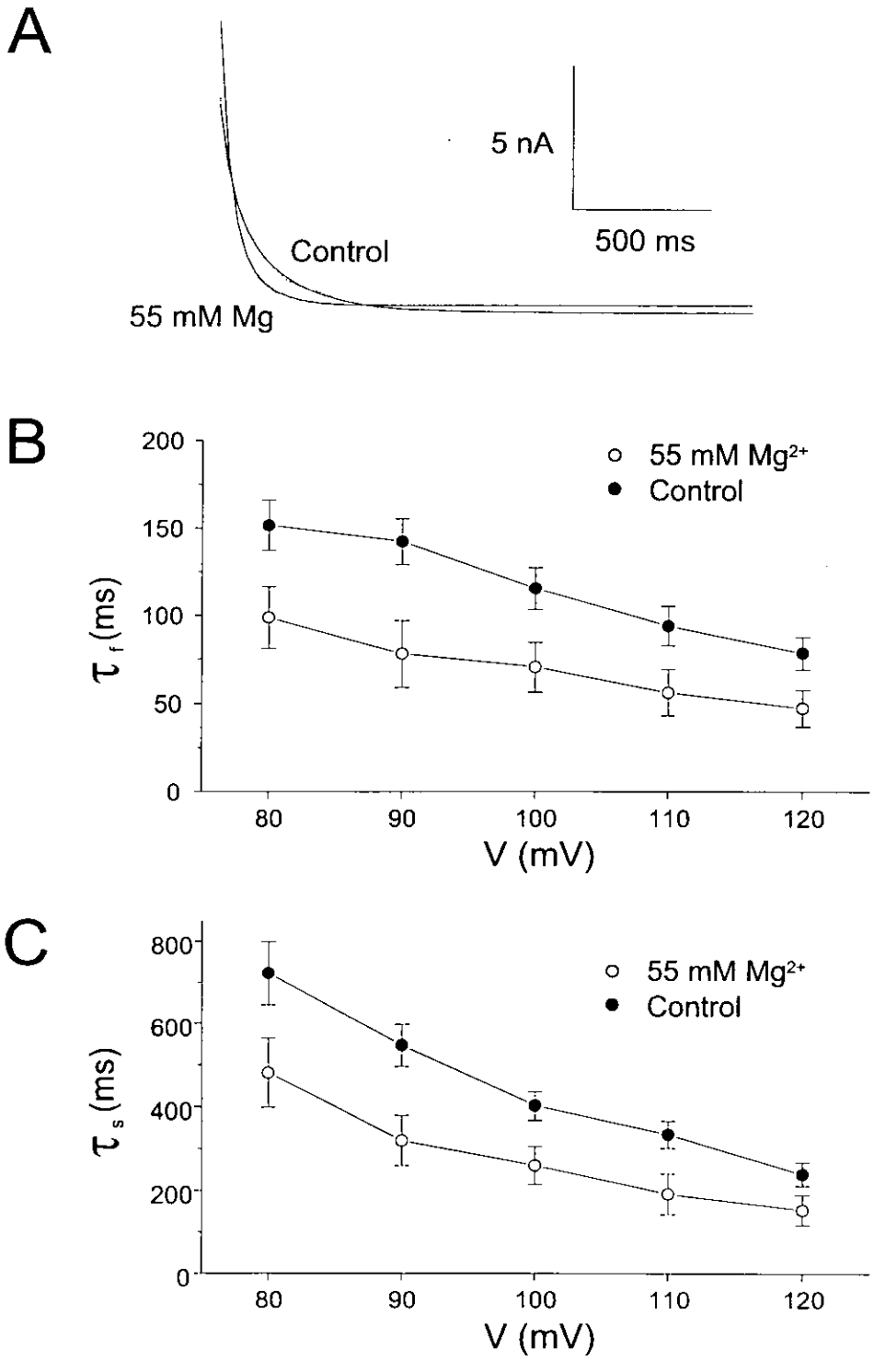
A
5 nA
500 ms
Control
55 mM Mg
B
200
150
100
50
0
τ_f (ms)
55 mM Mg^{2+}
Control
80
90
100
110
120
V (mV)
C
800
600
400
200
0
τ_s (ms)
55 mM Mg^{2+}
Control
80
90
100
110
120
V (mV)

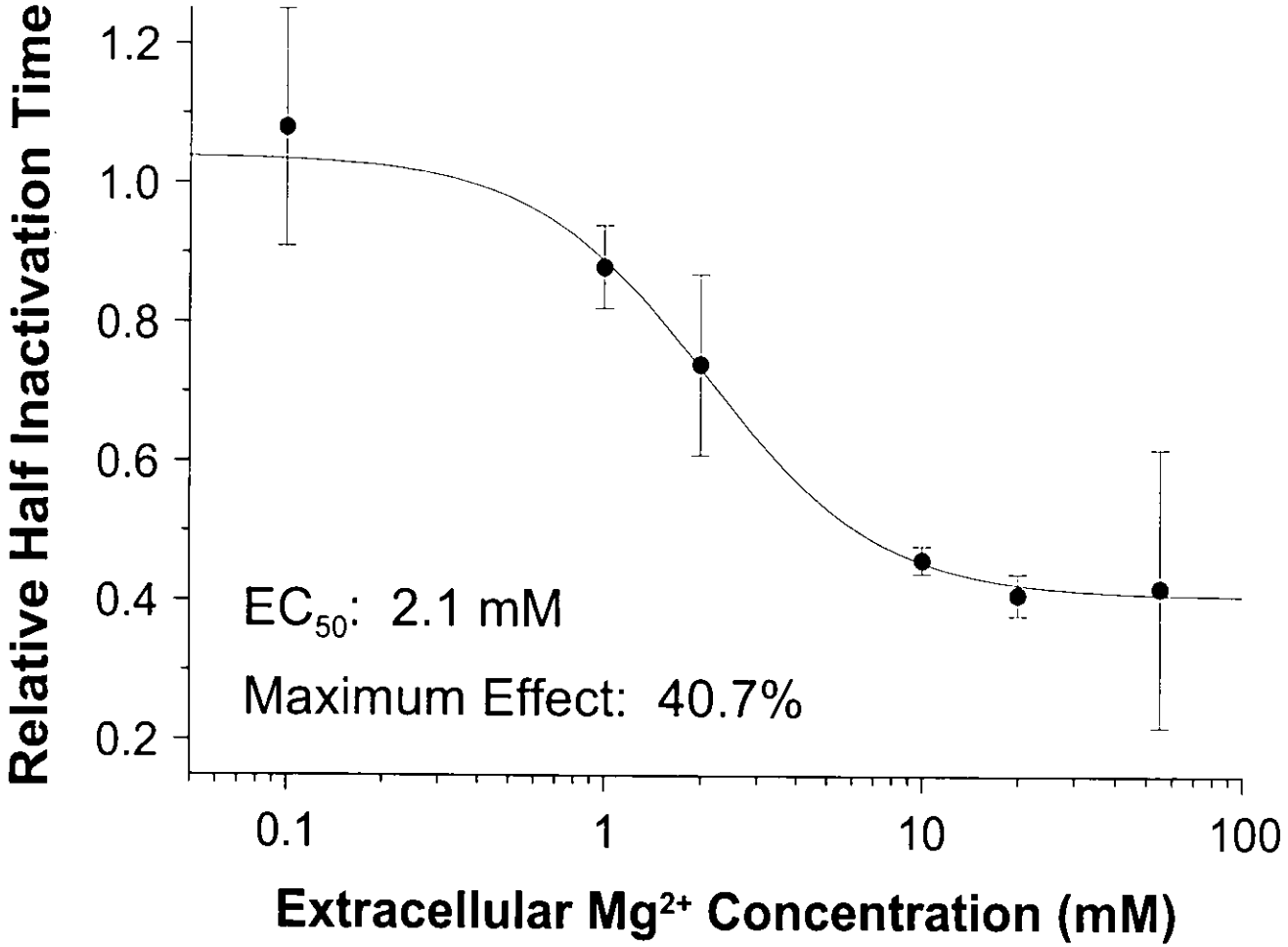
Relative Half Inactivation Time
1.2
1.0
0.8
0.6
0.4
0.2
EC50: 2.1 mM
Maximum Effect: 40.7%
0.1
1
10
100
Extracellular Mg2+ Concentration (mM)

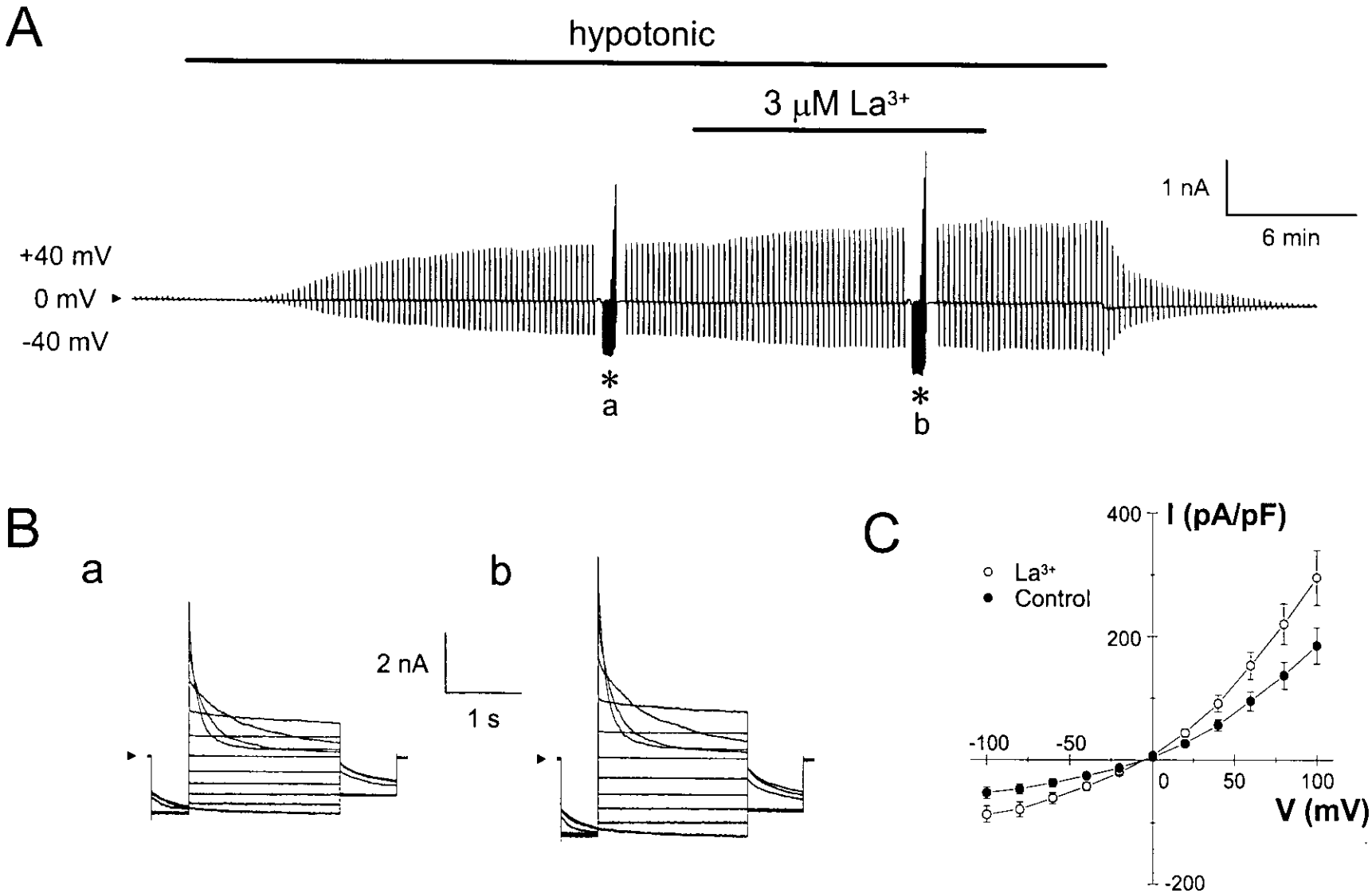
A
hypotonic
3 μM La3+
1 nA
6 min
+40 mV
0 mV
-40 mV
*
a
*
b
B
a
b
2 nA
1 s
C
400
I (pA/pF)
La3+
Control
200
-100
-50
0
50
100
V (mV)
-200

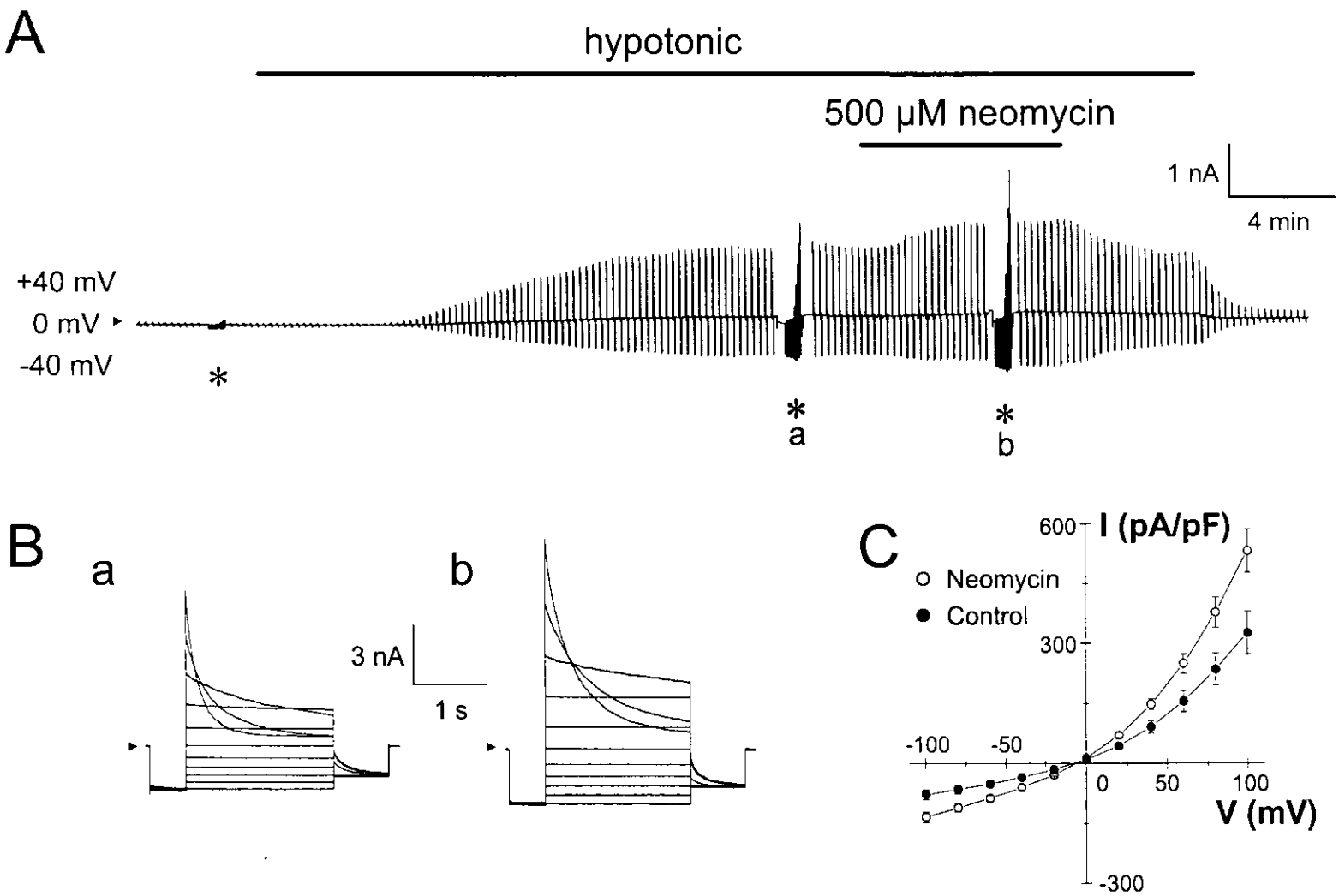
A
hypotonic
500 µM neomycin
1 nA
4 min
+40 mV
0 mV
-40 mV
*
*
a
*
b
B
a
b
3 nA
1 s
C
I (pA/pF)
600
300
-300
Neomycin
Control
-100
-50
0
50
100
V (mV)

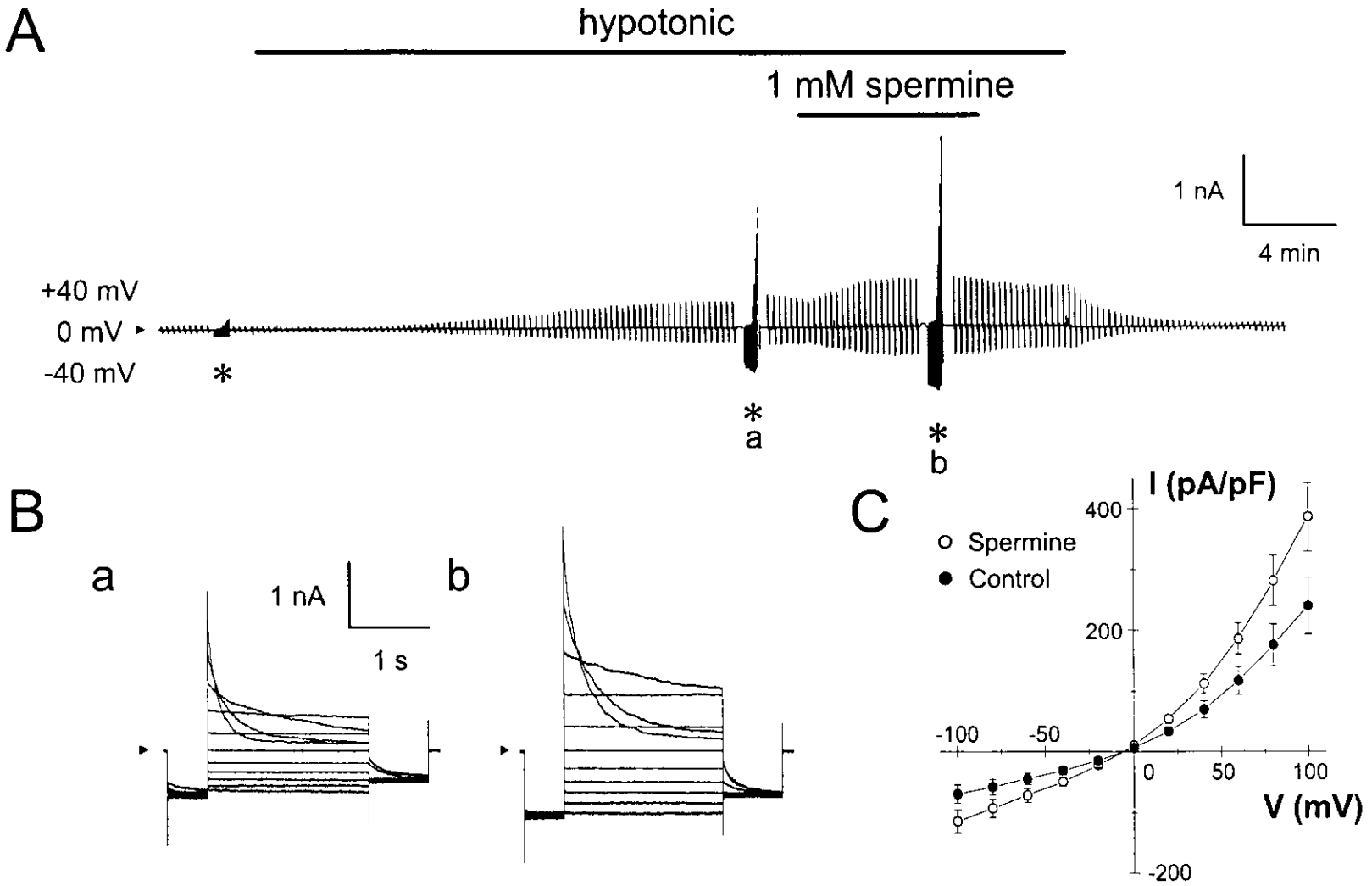
A
hypotonic
1 mM spermine
1 nA
4 min
+40 mV
0 mV
-40 mV
*
*
a
*
b
B
a
1 nA
1 s
b
C
I (pA/pF)
Spermine
Control
400
200
-100
-50
0
50
100
V (mV)
-200

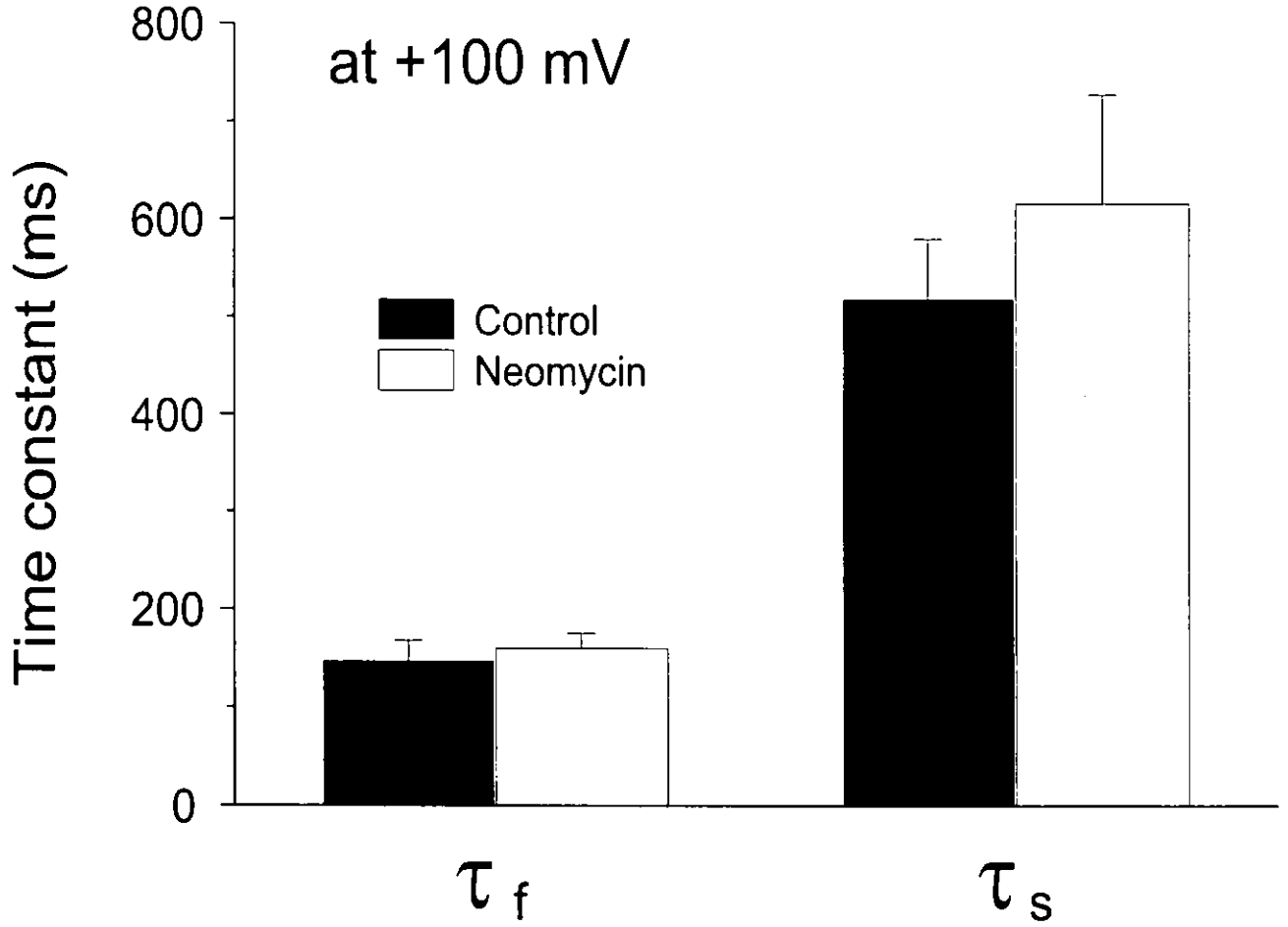
800
600
400
200
0
Time constant (ms)
at +100 mV
Control
Neomycin
τ f
τ s

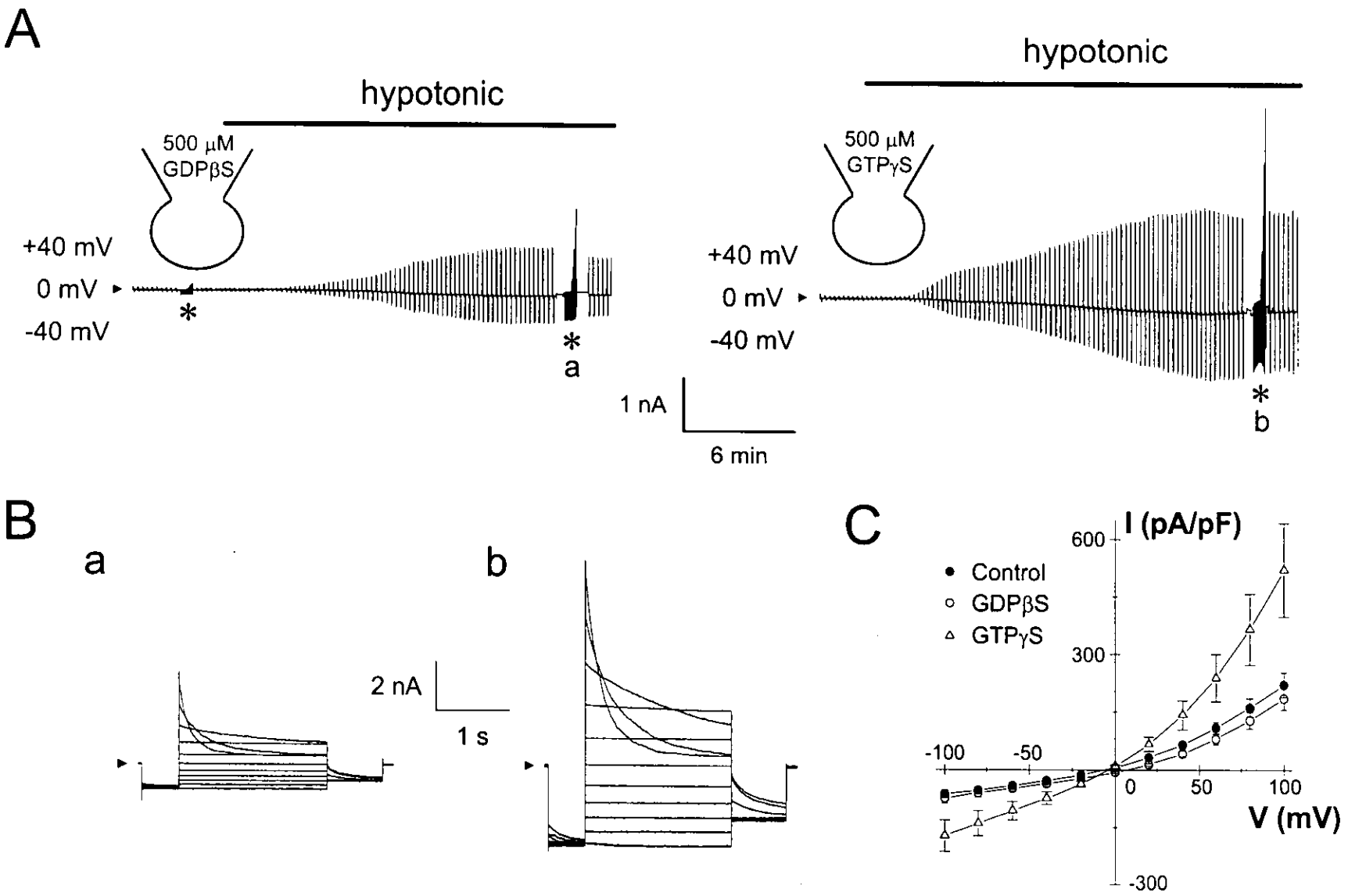
A
hypotonic
500 μM
GDPβS
+40 mV
0 mV
-40 mV
a
hypotonic
500 μM
GTPγS
+40 mV
0 mV
-40 mV
b
1 nA
6 min
B
a
b
2 nA
1 s
C
I (pA/pF)
600
300
-300
Control
GDPβS
GTPγS
-100
-50
0
50
100
V (mV)

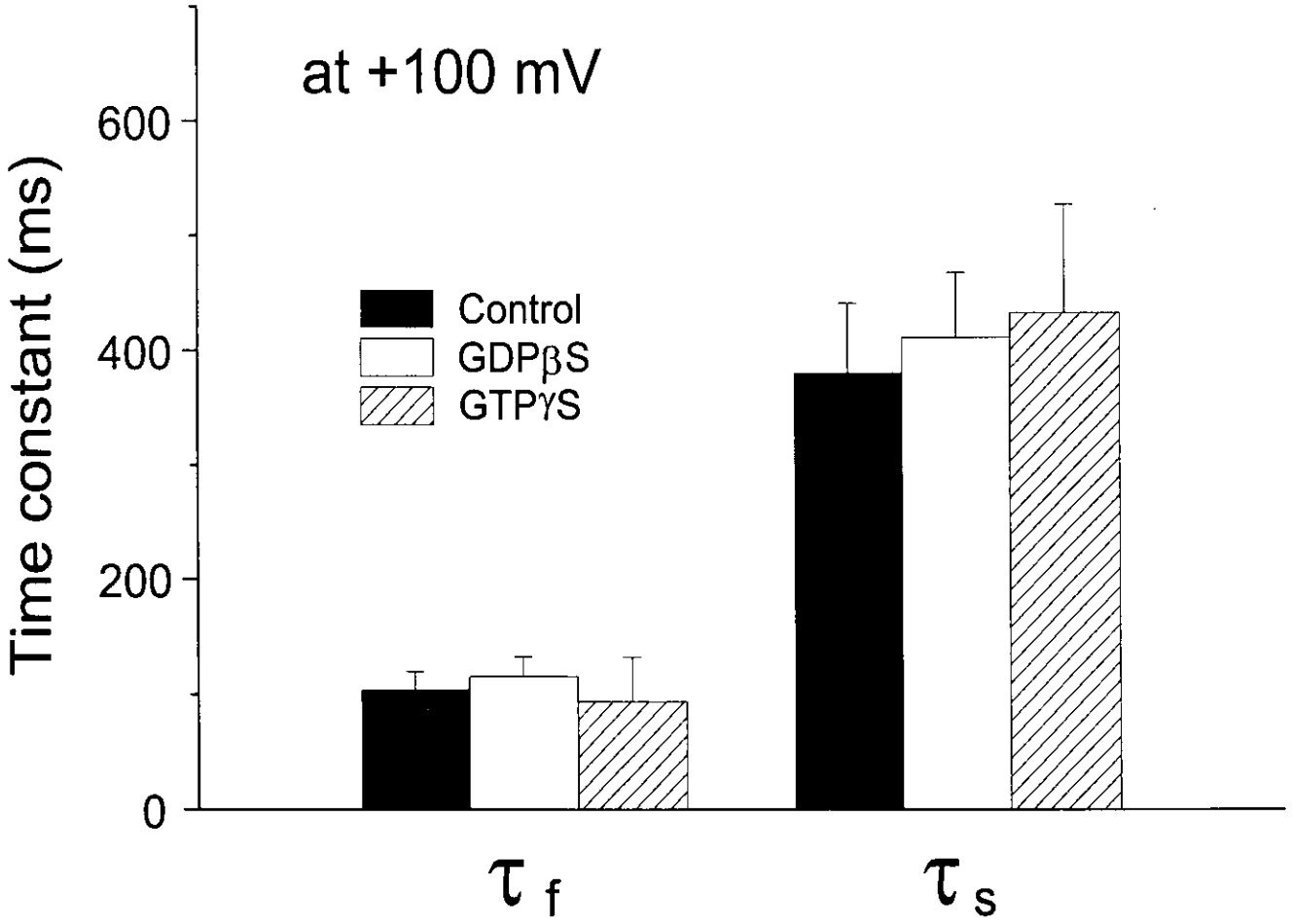
at +100 mV
Time constant (ms)
600
400
200
0
Control
GDPβS
GTPγS
τ f
τ s

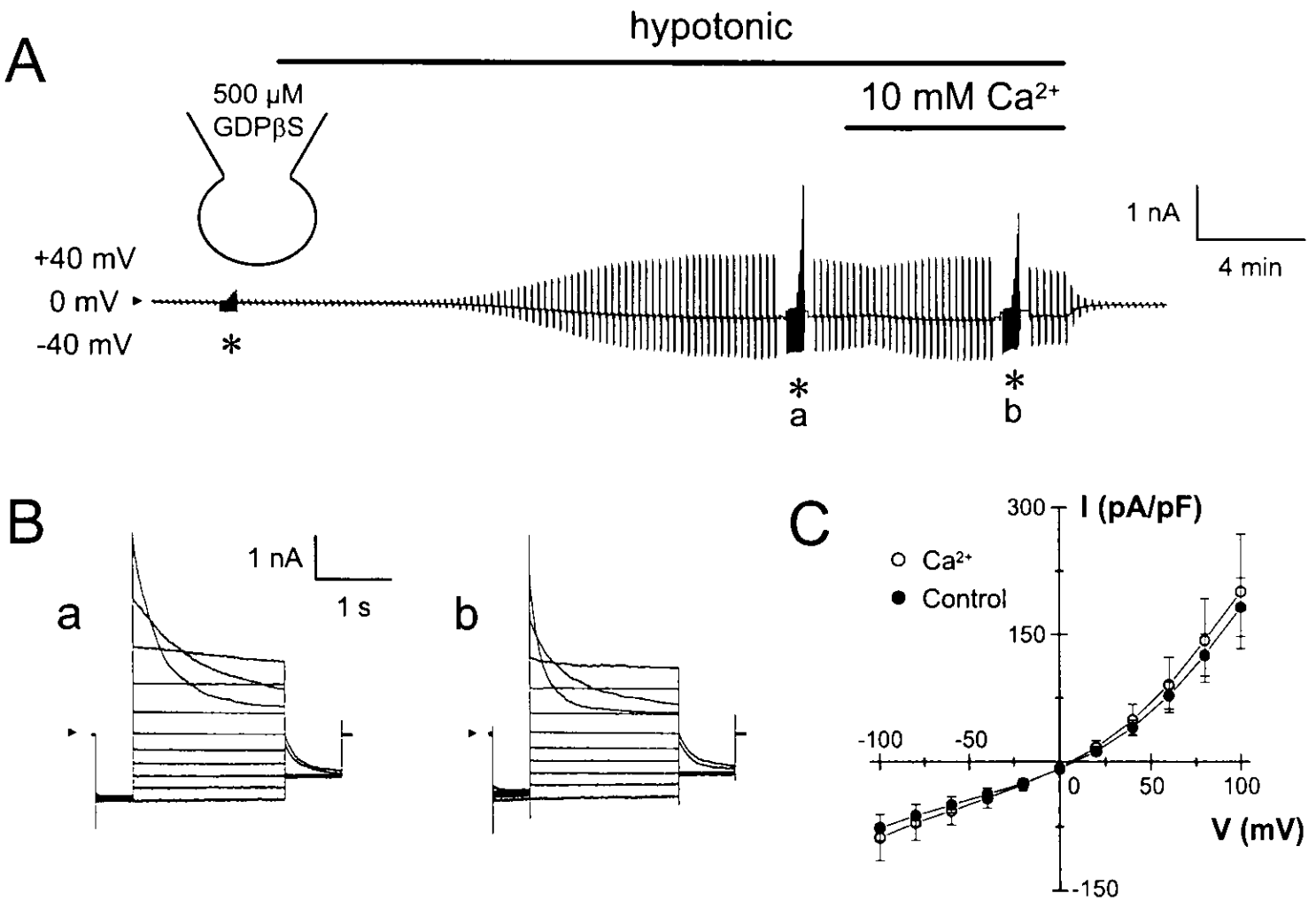
A
hypotonic
500 µM
GDPβS
10 mM Ca2+
1 nA
4 min
+40 mV
0 mV
-40 mV
a
b
B
1 nA
1 s
a
b
C
300
I (pA/pF)
Ca2+
Control
150
-100
-50
0
50
100
V (mV)
-150

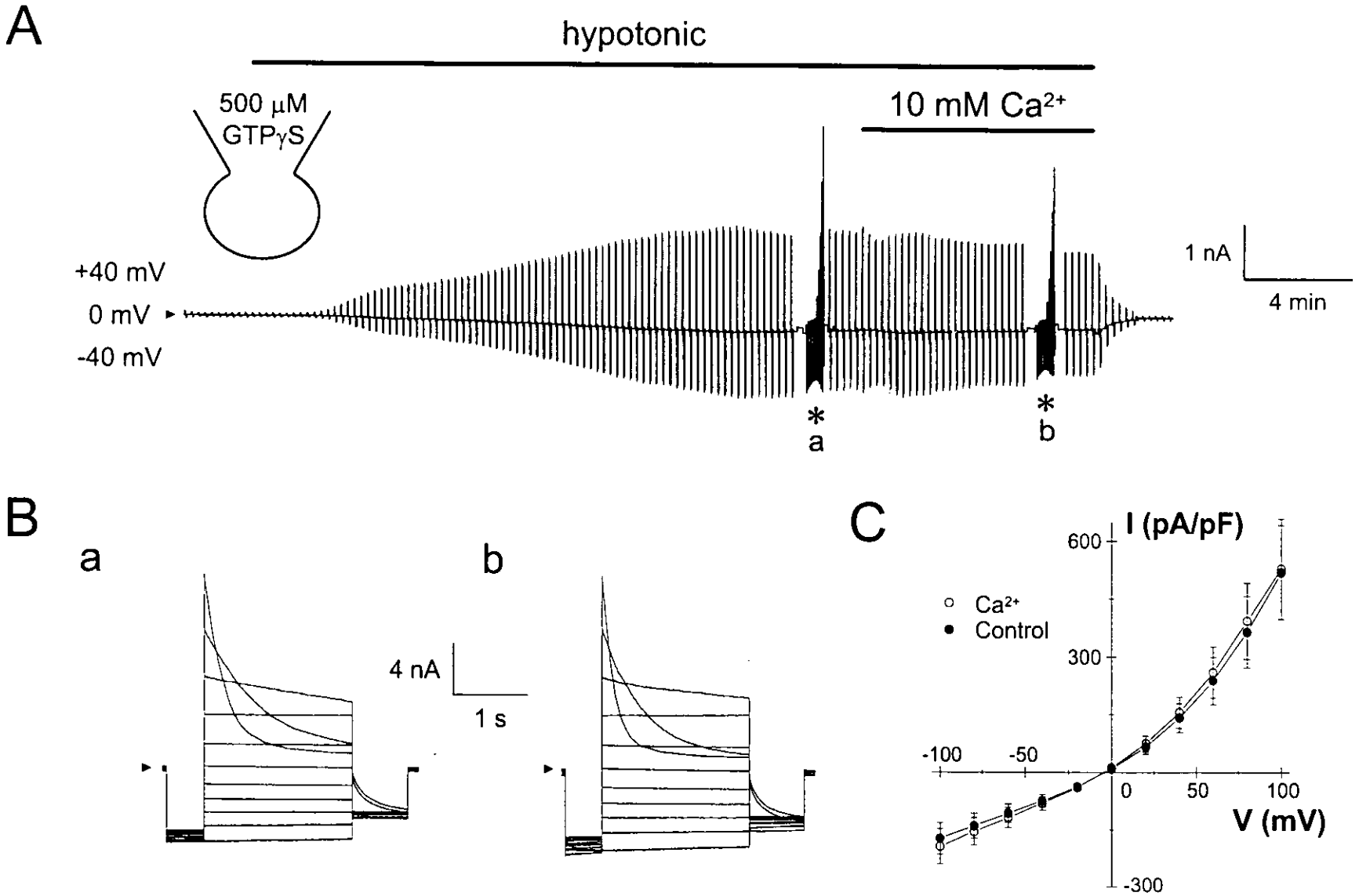
A
hypotonic
500 μM
GTPγS
10 mM Ca2+
+40 mV
0 mV
-40 mV
1 nA
4 min
*
a
*
b
B
a
b
4 nA
1 s
C
I (pA/pF)
600
300
-300
Ca2+
Control
-100
-50
0
50
100
V (mV)

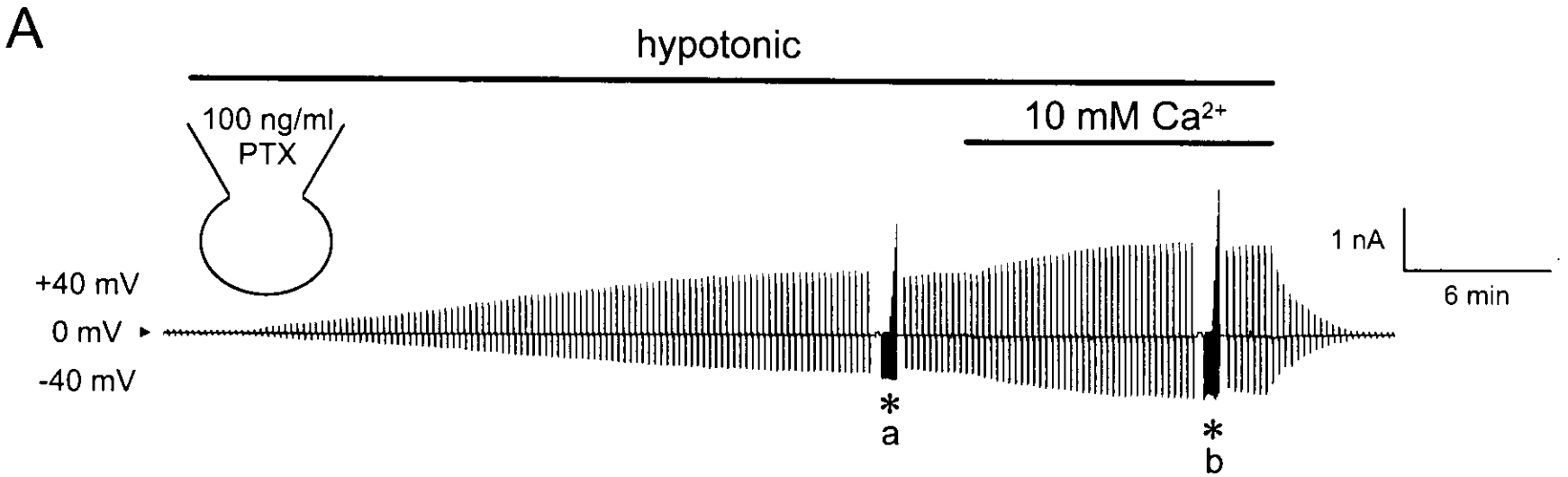
A
hypotonic
100 ng/ml
PTX
10 mM Ca2+
+40 mV
0 mV
-40 mV
1 nA
6 min
*
a
*
b

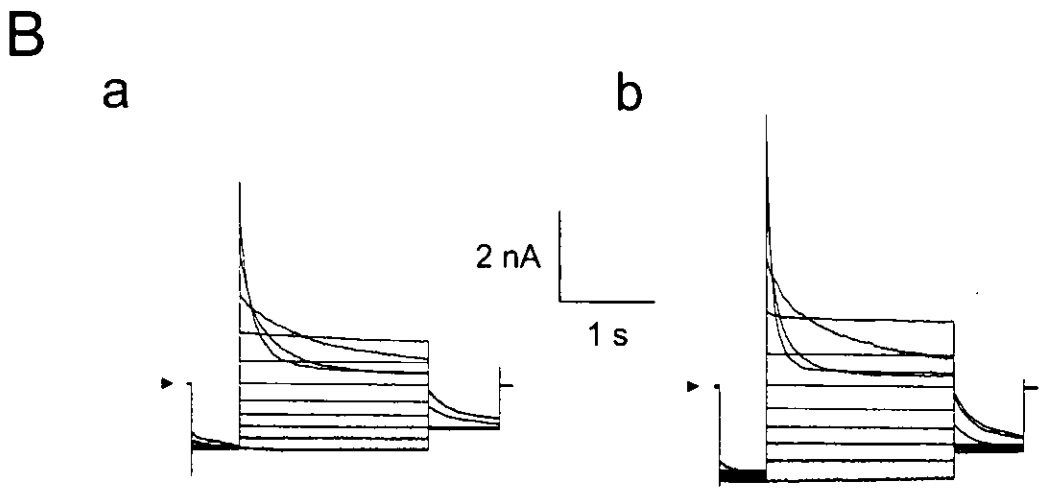
B
a
b
2 nA
1 s

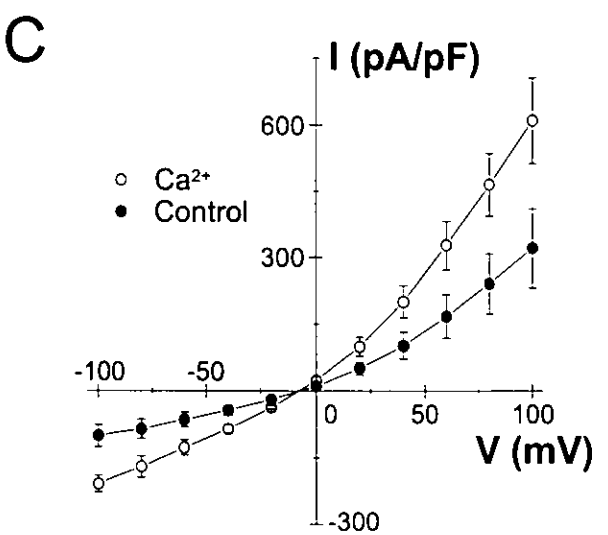
C
I (pA/pF)
600
300
-300
Ca2+
Control
-100
-50
0
50
100
V (mV)

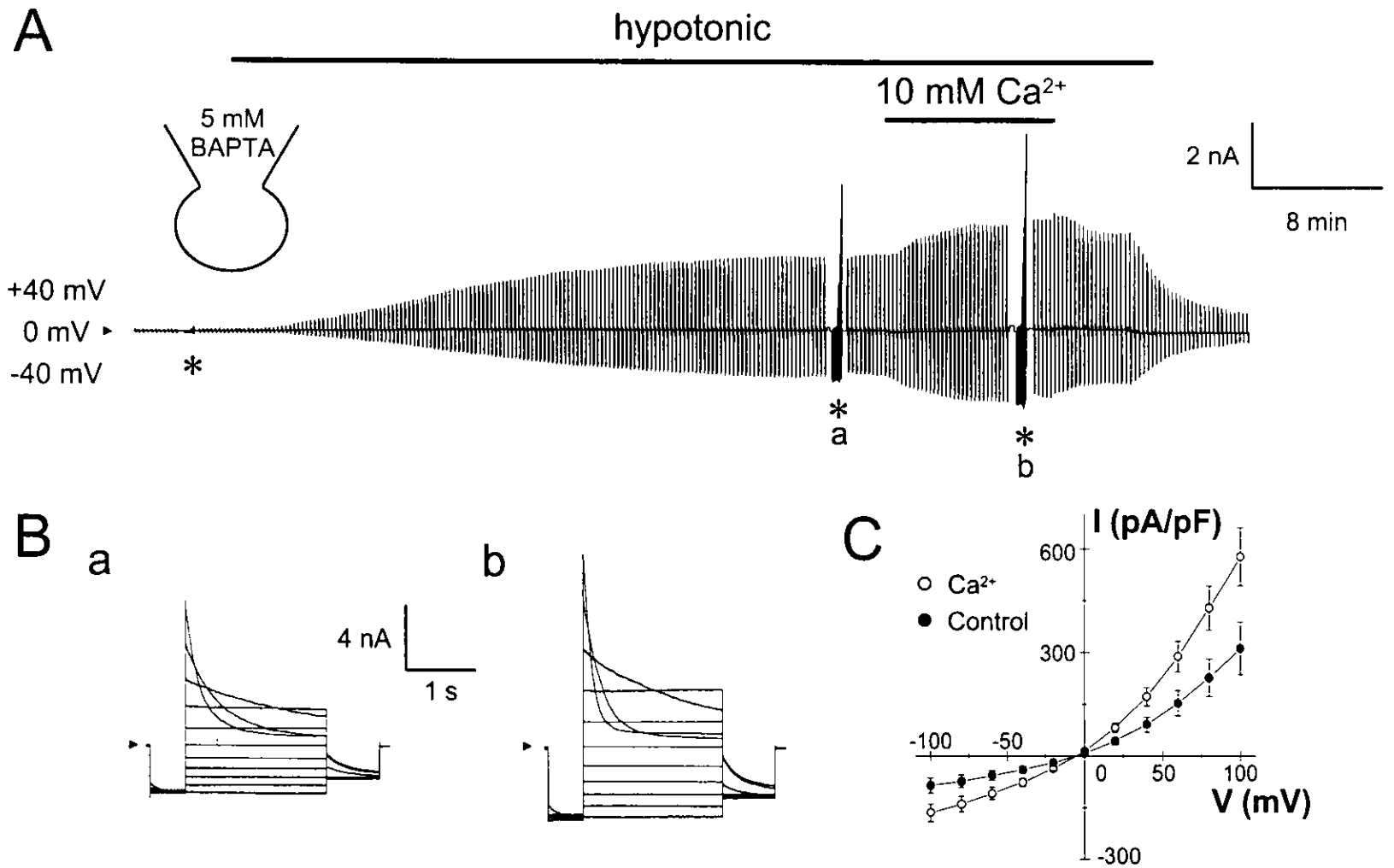
A
hypotonic
10 mM Ca2+
5 mM
BAPTA
2 nA
8 min
+40 mV
0 mV
-40 mV
*
*
a
*
b
B
a
b
4 nA
1 s
C
I (pA/pF)
Ca2+
Control
600
300
-100
-50
0
50
100
V (mV)
-300

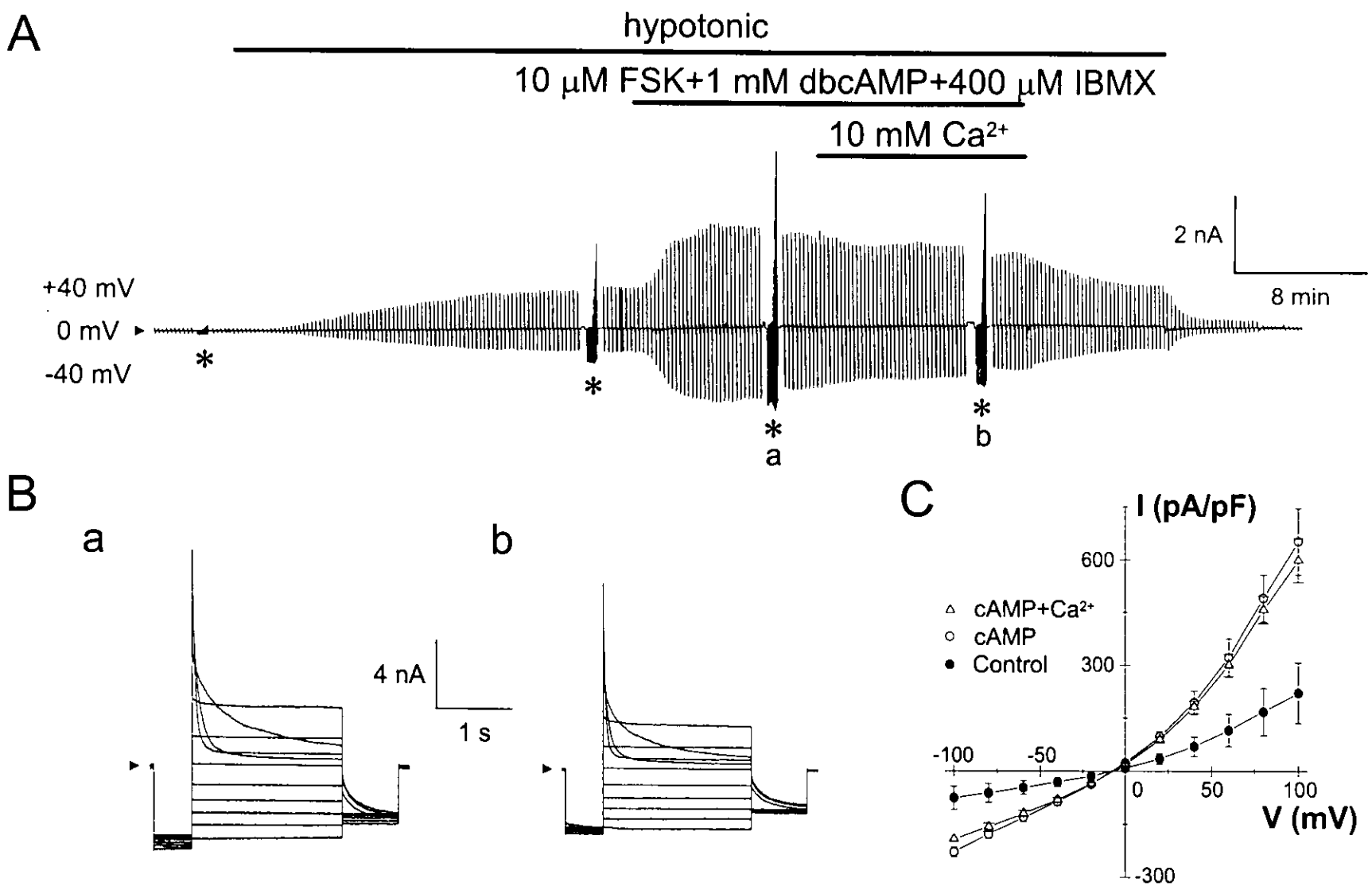
A
hypotonic
10 μM FSK+1 mM dbcAMP+400 μM IBMX
10 mM Ca2+
2 nA
8 min
+40 mV
0 mV
-40 mV
a
b
B
a
b
4 nA
1 s
C
I (pA/pF)
600
300
-300
cAMP+Ca2+
cAMP
Control
-100
-50
0
50
100
V (mV)

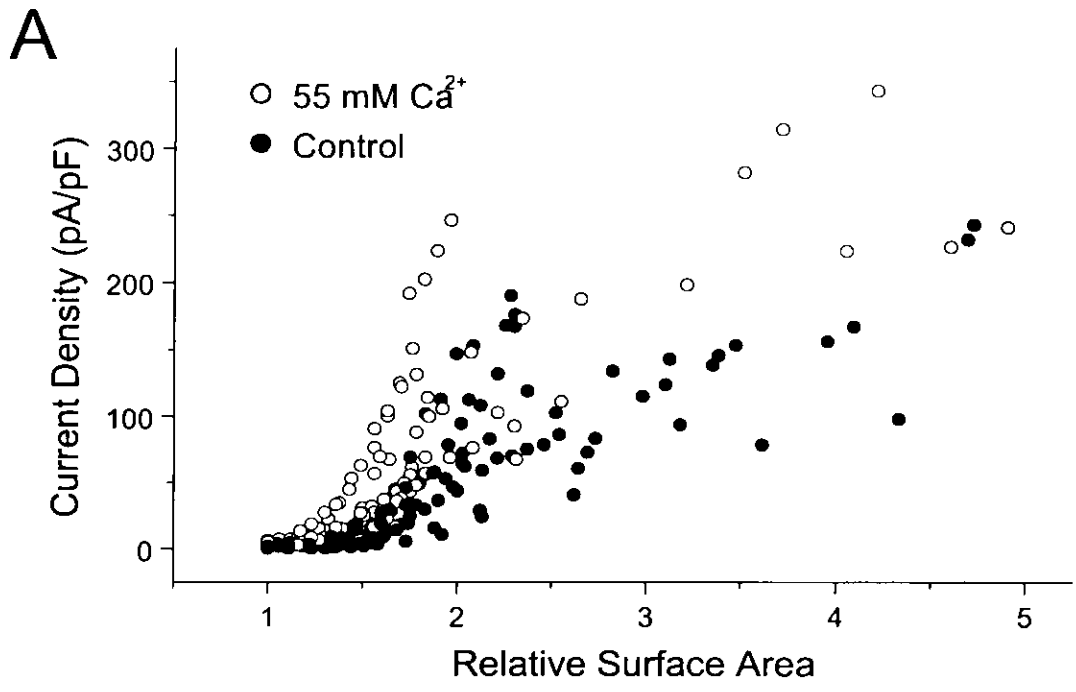
A
55 mM Ca2+
Control
Current Density (pA/pF)
300
200
100
0
1
2
3
4
5
Relative Surface Area

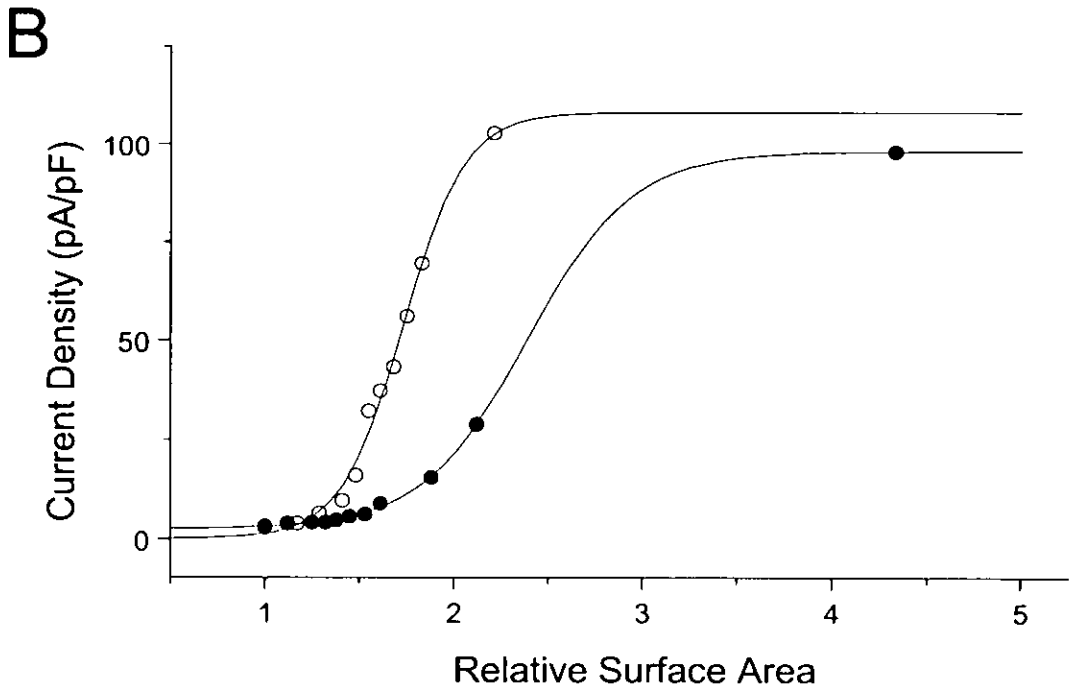
B
Current Density (pA/pF)
100
50
0
1
2
3
4
5
Relative Surface Area